



**HAL**  
open science

**The Last Termination in the South Indian Ocean: A unique terrestrial record from Kerguelen Islands (49°S) situated within the Southern Hemisphere westerly belt**

Nathalie van Der Putten, Cyriel Verbruggen, Svante Björck, Elisabeth Michel, Jean-Robert Disnar, Emmanuel Chapron, Bertrand N. Moine, Jacques-Louis de Beaulieu

► **To cite this version:**

Nathalie van Der Putten, Cyriel Verbruggen, Svante Björck, Elisabeth Michel, Jean-Robert Disnar, et al.. The Last Termination in the South Indian Ocean: A unique terrestrial record from Kerguelen Islands (49°S) situated within the Southern Hemisphere westerly belt. *Quaternary Science Reviews*, 2015, 122, pp.142-157. 10.1016/j.quascirev.2015.05.010 . insu-01165120

**HAL Id: insu-01165120**

**<https://insu.hal.science/insu-01165120>**

Submitted on 19 Jan 2017

**HAL** is a multi-disciplinary open access archive for the deposit and dissemination of scientific research documents, whether they are published or not. The documents may come from teaching and research institutions in France or abroad, or from public or private research centers.

L'archive ouverte pluridisciplinaire **HAL**, est destinée au dépôt et à la diffusion de documents scientifiques de niveau recherche, publiés ou non, émanant des établissements d'enseignement et de recherche français ou étrangers, des laboratoires publics ou privés.



Contents lists available at ScienceDirect

# Quaternary Science Reviews

journal homepage: [www.elsevier.com/locate/quascirev](http://www.elsevier.com/locate/quascirev)

## The Last Termination in the South Indian Ocean: A unique terrestrial record from Kerguelen Islands (49°S) situated within the Southern Hemisphere westerly belt



Nathalie Van der Putten<sup>a,\*</sup>, Cyriel Verbruggen<sup>b</sup>, Svante Björck<sup>a</sup>, Elisabeth Michel<sup>c</sup>, Jean-Robert Disnar<sup>d</sup>, Emmanuel Chapron<sup>d,1</sup>, Bertrand N. Moine<sup>e</sup>, Jacques-Louis de Beaulieu<sup>f</sup>

<sup>a</sup> Department of Geology, Quaternary Sciences, Lund University, Sölvegatan 12, 223 64 Lund, Sweden

<sup>b</sup> Department of Geology and Soil Science, Ghent University, Krijgslaan 281 (S8), 9000 Gent, Belgium

<sup>c</sup> Laboratoire des Sciences du Climat et de l'Environnement (LSCE), Laboratoire mixte CNRS-CEA-UVSQ, Avenue de la Terrasse, 91198 Gif-sur-Yvette Cedex, France

<sup>d</sup> Institut des Sciences des la Terre d'Orléans, ISTO, UMR 7327, CNRS, Univ Orléans, BRGM, 1A rue de la Férollerie, 45071 Orléans Cedex 2, France

<sup>e</sup> Universités de Lyon, Université Jean Monnet, Laboratoire Magmas et Volcans UMR-CNRS 6524, 42023 Saint-Etienne, France

<sup>f</sup> IMBE-UMR CNRS 7263/IRD/Aix-Marseille Université 237, Europôle Méditerranéen de l'Arbois, BP 80, 13545 Aix-en-Provence Cedex 04, France

### ARTICLE INFO

#### Article history:

Received 23 September 2014

Received in revised form

6 May 2015

Accepted 12 May 2015

Available online 10 June 2015

#### Keywords:

Palaeoclimatology

Last Termination

Peat record

Kerguelen Islands

Southern Ocean

Indian Ocean

Oceanic Cold Reversal

Southern Hemisphere westerly belt

### ABSTRACT

The awareness of the significance of the Southern Ocean in the Earth's climate system has become increasingly obvious. The deglacial atmospheric CO<sub>2</sub> rise during warming periods in Antarctica has been attributed to CO<sub>2</sub> ventilation from the deep ocean caused by enhanced upwelling around the Antarctic Divergence. It has been hypothesized that, more intense Southern Hemisphere westerly winds aligned with the Antarctic Circumpolar Current due to a southward shift of the wind belt from its Last Glacial Maximum equator-ward position, are the main drivers. Reconstructions of past changes in atmospheric circulation in the Southern Hemisphere are still scarce and the overall picture is patchy with sometimes contradictory results. For obvious reasons, most terrestrial records originate from southern South America and New Zealand. Here we present a terrestrial record from the Indian sector of the Southern Ocean, from Kerguelen Islands located at 49°S. A peat record is investigated using a multi-proxy approach (pollen and plant macrofossils, magnetic susceptibility, XRF analyses, biogenic silica content, Rock-Eval6 analysis and humification degree). Peat accumulation starts at about 16,000 cal yr BP with relatively warm and dry conditions. The most prominent change in our proxy data occurs at 13,600 cal yr BP, when peat ponds were established on the peat surface, resulting in lacustrine-type deposits, as a result of very high humidity, and with proxies implying very windy conditions. Within chronological uncertainties, this onset coincides with the onset of the so-called Oceanic Cold Reversal, based on the deuterium excess data in the EPICA Dome C ice core record. Kerguelen Islands are located in the moisture source area of Dome C and a change in atmospheric circulation at that time could explain both records. Around 12,900 cal yr BP, at the end of the Antarctic Cold Reversal, pond/lake sediments give way to more peaty deposits, with proxies suggesting slightly drier, less windy and probably warmer conditions. Kerguelen Islands became less influenced by the Southern Hemisphere westerly winds and these conditions were amplified during the early Holocene climate optimum as found in Antarctic ice core records.

© 2015 Elsevier Ltd. All rights reserved.

## 1. Introduction

It is known from Greenland ice core records that, during the Last Termination (c. 22,000–11,500 cal yr BP after Lowe et al., 2008), the North Atlantic region was characterized by a sudden return to cold conditions, a period/event called the Younger Dryas (YD)/GS 1

\* Corresponding author.

E-mail address: [Nathalie.van\\_der\\_putten@geol.lu.se](mailto:Nathalie.van_der_putten@geol.lu.se) (N. Van der Putten).

<sup>1</sup> Present address: GEODE, UMR5602, Université Toulouse 2 Jean Jaures, Maison de la recherche, 5 allée Antonio Machado, 31058 Toulouse Cedex 1, France.

(12,900–11,700 cal yr BP), after an initial abrupt warming during the Bølling–Allerød/GI-1 period/events (14,700–12,900 cal yr BP) (Lowe et al., 2008). In comparison, temperature changes in Antarctica are more gradual. Cold events in Greenland correlate with periods of warming in Antarctica and *vice versa*, related to the ‘bipolar seesaw’ mechanism (Broecker, 1998; Stenni et al., 2011). In Antarctica, deglacial warming starts at about 18,350 cal yr BP, culminating in the Antarctic Isotopic Maximum 1 (AIM 1, Stenni et al., 2011; Veres et al., 2013), and was interrupted by a return to colder conditions, or a pause in the warming, during the Antarctic Cold Reversal (ACR, 14,650–12,900 cal yr BP) after which a second warming occurred and continued into the Holocene. Based on deuterium-excess data from the EPICA Dome C ice record (EDC), Stenni et al. (2001) report an Oceanic Cold Reversal (OCR) in the moisture-source area for precipitation of EDC, which is the South Indian Ocean, with an onset about 1000 years later than the ACR. Whether the OCR is related to a change in sea surface temperature in the source area or a shift in the moisture source itself, due to a change in atmospheric circulation at basin scale is not yet clear (Stenni et al., 2011).

Outside the Antarctic continent, in the mid latitudes of the Southern Hemisphere (SH), palaeoclimatic records in general and terrestrial ones in particular, are still sparse in comparison with the same latitudes in the Northern Hemisphere. However, during the last decades, there has been a reinforced effort to reconstruct past environmental and climatic changes in the SH mid latitudes. One of the questions that has received considerable attention is whether SH mid latitudes show an Antarctic or a Northern Hemisphere palaeoclimatic signature: for example, was the YD a global or Northern Hemisphere (NH) climate event (e.g. Bennett et al., 2000; Andres et al., 2003; Williams et al., 2005; Barrows et al., 2007). Some SH records reveal cooling events which are synchronous with the NH YD cooling such as in the Taylor Dome ice core record (Steig et al., 1998) and a marine record south (34°S) of Australia (Andres et al., 2003) challenging the bipolar seesaw hypothesis. In the case of the Taylor Dome ice core, the integrity of the time scale has been questioned (Stenni et al., 2011) and in a marine setting, one has to take into account the marine reservoir age, especially during the Last Termination when changes in ocean circulation resulted in possibly fluctuating reservoir ages (Siani et al., 2013). Lately, a growing consensus is that the southern mid-latitudes show an Antarctic palaeoclimatic signature (e.g. Denton et al., 2010), although its northern limit is uncertain. A second research topic that has received extensive attention is the role of the Southern Ocean (SO) and related to this, shifts of the Southern Hemisphere westerly belt (SHW), in releasing CO<sub>2</sub> from the deep ocean during warming phases in Antarctica (Toggweiler et al., 2006; Anderson et al., 2009; Denton et al., 2010; Lamy et al., 2010; Siani et al., 2013). A conceptual model has been presented by Toggweiler et al. (2006) suggesting a pole-ward shift of the SHW from its equator-ward Last Glacial Maximum (LGM) position, aligning the SHW with the Antarctic Circumpolar Current (ACR), favouring ventilation of CO<sub>2</sub> to the atmosphere around Antarctica at the Antarctic divergence. Anderson et al. (2009), hypothesize that during cold periods in the North Atlantic, the Inter-tropical Convergence Zone (ITCZ) has a more southward location, pushing the SHW southward resulting in increased CO<sub>2</sub> ventilation and warming in Antarctica. Denton et al. (2010) invoke a reduced Atlantic Meridional Overturning Circulation (AMOC) followed by expanded sea ice in the North Atlantic, and in consequence a higher seasonality, as the way to spread cold events throughout the North Atlantic and the tropics, with a southward shift of the ITCZ (weakening of the Asian Monsoon) and the SHW as a result.

In relation to the LGM equator-ward location of the SHW, a recent proxy data comparison, highlighted that an equator-ward

shift or strengthening of the SHW could explain much of the proxy records, but that other processes could also be involved (Kohfeld et al., 2013). In a follow-up study, a modelling approach was used together with a model-data comparison (Sime et al., 2013). None of the models that reproduce realistic LGM moisture/precipitation data – the most common used proxy for reconstructing changes in SHW – show a large equator-ward shift in the SHW.

We therefore think that more proxy data based evidence is needed to test the different hypotheses on mechanisms and internal feedbacks of the climate system in relation to latitudinal shifts and/or strengthening of the SHW, changing ocean circulation, CO<sub>2</sub> out-gassing and changing temperature in Antarctica and the SH mid latitudes.

The SH mid latitudes constitute the SO, with southern South America, and to a lesser extent New Zealand, as the main land areas. In consequence the vast majority of the terrestrial proxy records originate from these areas. However, dispersed in the SO, islands and island groups occur, which can be targeted as a potential source for terrestrial palaeoclimatic archives. Here we present the results of a multi-proxy study of a 16 000 year old peat sequence from Kerguelen Islands, a sub-Antarctic archipelago located at 49°S in the Indian Ocean, situated in the moisture-source area of the EDC ice core record. In this paper we will concentrate on the Last Termination focussing on the following questions: (i) how did climate evolve during the Last Termination in the Indian sector of the SO, (ii) did any cold reversal occur at Kerguelen Islands and if so, what is its timing, (iii) how does the climate history relate to the climate reconstructions from the EDC ice core, and (iv) can we relate our results to changes (latitudinal shifts and/or strengthening/weakening) of the SHW?

## 2. Study area

The Kerguelen archipelago (49°S–69°E, Fig. 1A and B) is a French island group in the South Indian Ocean. The main island, with an area of c. 7200 km<sup>2</sup>, is by far the largest of the sub-Antarctic islands (*sensu* Lewis-Smith, 1984) and is surrounded by numerous smaller islands. The archipelago is an emerged part of the vast Kerguelen-Gaussberg oceanic plateau and is of volcanic origin, dominated by basaltic lava flows. The western part of the main island is mountainous (with a mean elevation around 800 m), while the eastern part (Péninsule Courbet) is flat and characterized by glacial and glaciofluvial deposits and landforms (Hall, 1984). The highest point is the Mont Ross volcano with an altitude of 1850 m asl. The minimum age of the first volcanic formations on Kerguelen Islands is about 40 Myr (Giret et al., 2003) and the volcanic activity still persists today in the Rallier du Baty Peninsula. A small ice cap with outlet glaciers occurs in the western part of the archipelago (Cook ice cap, Fig. 1B) covering c. 12% of the island (Giret et al., 2003; Van der Putten et al., 2010). However, based on the presence of U-shaped valleys, moraines and fjords, it is clear that ice-cover was much larger in the past, but the exact extent and timing of previous glaciations is poorly constrained. Some studies suggest that these glacial landforms are not of LGM age and that the ice extent at that time was rather restricted (e.g. Nougier, 1970). In contrast, Hall (1984) suggested a more extensive ice-cover during the LGM with an equilibrium line altitude of c. 200 m. The timing of the last deglaciation is also not well known and is mainly based on a few basal radiocarbon dates of peat deposits (Hodgson et al., 2014; Van der Putten et al., 2010).

Nowadays, the Kerguelen archipelago is situated in the core of the SHW, within the Antarctic Circumpolar Current (ACC), at the Polar Front (PF) (Fig. 1A). This makes it a valuable site for reconstructing past changes in atmospheric and oceanic circulation

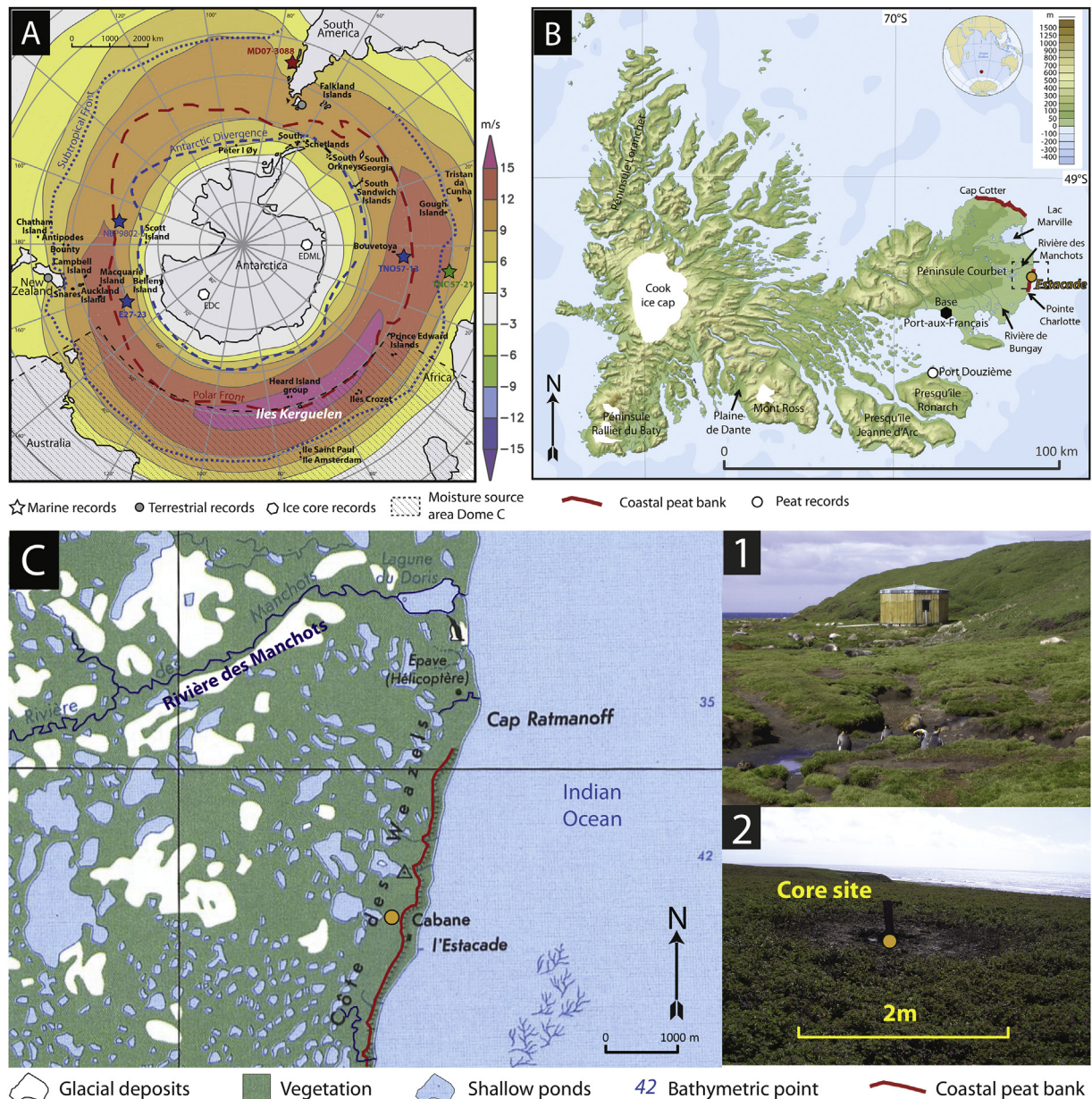


**Fig. 1.** (A) Map of the Southern Hemisphere high and mid-latitudes with the location of Kerguelen Islands (white bold italic), the oceanic fronts and the mean annual zonal winds (m/s) at 850 mb averaged for the period 1979–2009 based on Re-analysis data (NCEP CFSR). Sites discussed in the text: marine records (blue taken from Anderson et al., 2009; green taken from Barker et al., 2009; red taken from Montade et al., 2013; Siani et al., 2013); terrestrial records taken from Putnam et al., 2010 and Björck et al., 2012. (B) Kerguelen Islands with location of the Estacade site and other locations mentioned in the text. Map adapted based on a map by Rémi Kaupp via Wikimedia Commons. ([http://commons.wikimedia.org/wiki/File:Kerguelen\\_topographic\\_blank\\_map.png](http://commons.wikimedia.org/wiki/File:Kerguelen_topographic_blank_map.png)). (C) Inset showing details on site topography of the Estacade record and geomorphic processes currently active. Picture (1) was taken at the foot of the peat bank, looking to the south, showing the hut with behind the “cliff”. Picture (2) shows the coring site, looking in northern direction. The present day vegetation on the site is dominated by *Acacia magellanica*. The inset is taken from the topographic map from IGN via the geoportal web site (<http://www.geoportail.gouv.fr/accueil>). (For interpretation of the references to colour in this figure legend, the reader is referred to the web version of this article.)

changes. Kerguelen Islands show a great diversity in landscapes and in potential terrestrial archives, such as lake sediments and peat deposits. Furthermore, the archipelago has not been directly affected by human presence until very recently (18th century) making it an excellent area to study past natural climate variability.

The climate of Kerguelen Islands is cool-oceanic with small seasonal differences and a mean annual temperature of +4.6 °C (Frenot et al., 2001). The mean temperature at sea level of the coldest month is 2 °C and permafrost is not present in peat deposits today. The mean annual precipitation is 800 mm (Frenot et al., 2001) and this seems to be rather low for a sub-Antarctic island, especially one that is situated in the core of the SHW. However, the

meteorological station is located in the eastern part of the island (Port-aux-Français, Fig 1B), on the lee side of the mountains, which results in an orographic effect. Annual precipitation in the western part of the archipelago can attain 3200 mm (Frenot et al., 2001). The mean wind velocity is about 10 m/s.

### 3. Material and methods

#### 3.1. Fieldwork

In November 2006–January 2007, fieldwork was conducted in the eastern part of the Kerguelen archipelago. Several sites were

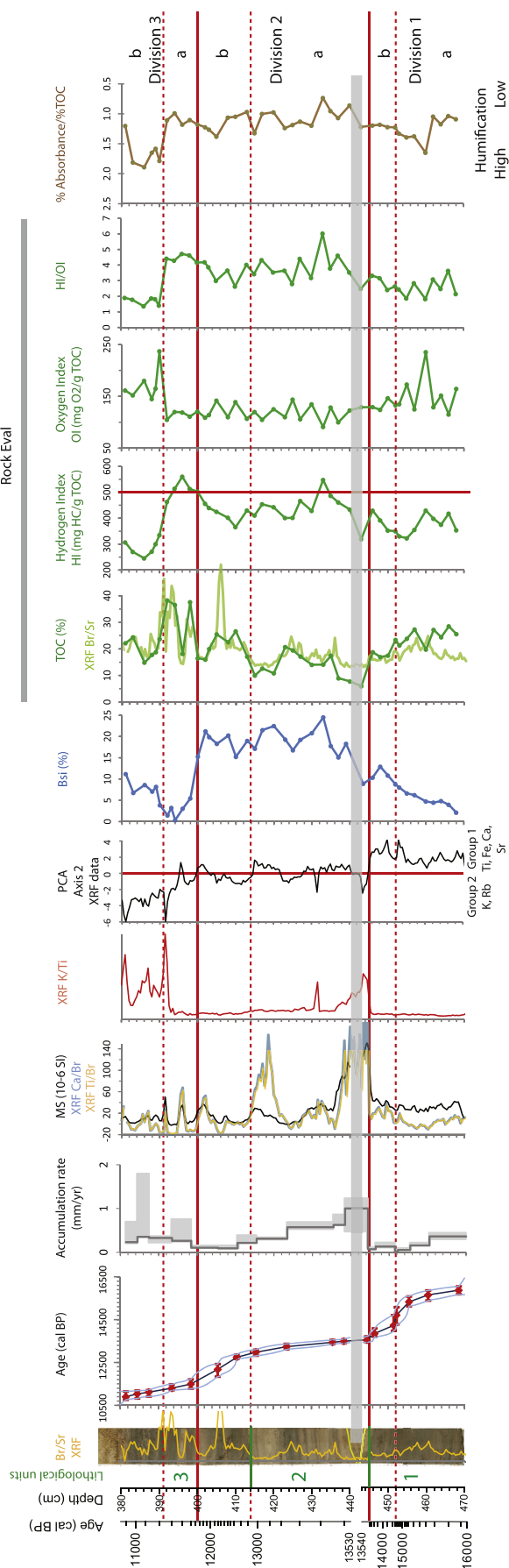


**Fig. 2.** Picture log, lithological units, the age–depth model ( $2\sigma$  error bars) and the accumulation rate (mm/yr) with the grey shading the accumulation rates calculated based on the  $2\sigma$  errors, together with selected proxy data: magnetic susceptibility (MS) plotted with the Ca/Br and Ti/Br ratios; the K/Ti ratio; the Br/Sr ratio; hydrogen index (HI), oxygen index (OI) and the HI/OI ratio; % Absorbance/% TOC ratio.

prospected with hand coring equipment, using a 4 cm diameter gouge auger, an excellent tool for coring peat deposits, in order to survey the thickness of the deposits and detect continuous organic sequences suitable for palaeoenvironmental research. The Estacade sequence was sampled by drilling in two 11.5 cm diameter CALYPSO PVC tubes. A first tube with a length of 277 cm was hammered down to a depth of 262 cm. With hand coring equipment deposits around the tube were retrieved in order to liberate it from the surrounding peat so that the tube could be lifted. A second tube of 498 cm length was put in the same hole and hammered to a depth of 470 cm, until it became impossible to get it further down. The same procedure was used to liberate and retrieve the second tube. In order to make sure that the base of the deposits was attained, the gouge auger was used and pushed down until it was stopped by a stony impenetrable deposit or bedrock. A sample of about 52 cm long was retrieved in the gouge auger and stored in a half 7.5 cm diameter PVC tube for transport. Slight compaction of the deposits of 5 cm was measured for the first tube, no compaction occurred in the second tube.

**3.2. Stratigraphy, rockmagnetic and geochemical analyses**

In the laboratory, the PVC tubes were split into two halves and the cores were described and photographed in increments of c. 20 cm length, in order to construct the picture log. It became clear that the 52 cm long sequence sampled with the gouge auger showed a nearly complete overlap with the lower parts of the sequence sampled with the CALYPSO tube except for 3 additional cm. A basal sample of the gouge auger sequence was submitted for  $^{14}\text{C}$  dating. Before subsampling the sequence in the CALYPSO tubes, magnetic susceptibility was measured with 5 mm resolution using a Bartington Instruments Ltd MS2E1 sensor and a TAMISCAN-TS1 automatic conveyer at Lund University, Sweden (Sandgren and Snowball, 2001).

The cores were consequently scanned with an ITRAX XRF Core Scanner from Cox Analytical Systems at the Department of Geological Sciences, Stockholm University, Sweden, using a Mo tube set at 30 kV and 25 mA with a dwell time of 100 s and a step size of 5 mm. The elemental data were normalized to the

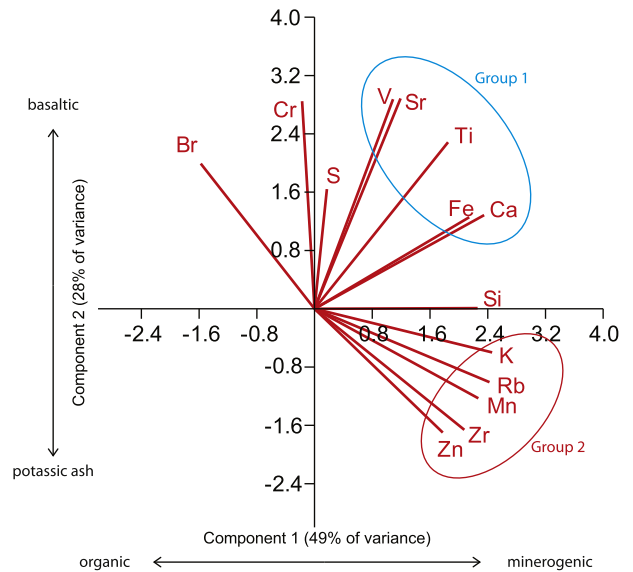


**Fig. 3.** Biplot of the principal component analysis of the major elements (XRF). Percentage of variance of component 1 and 2 are shown on the axis together with the interpretation of the components.

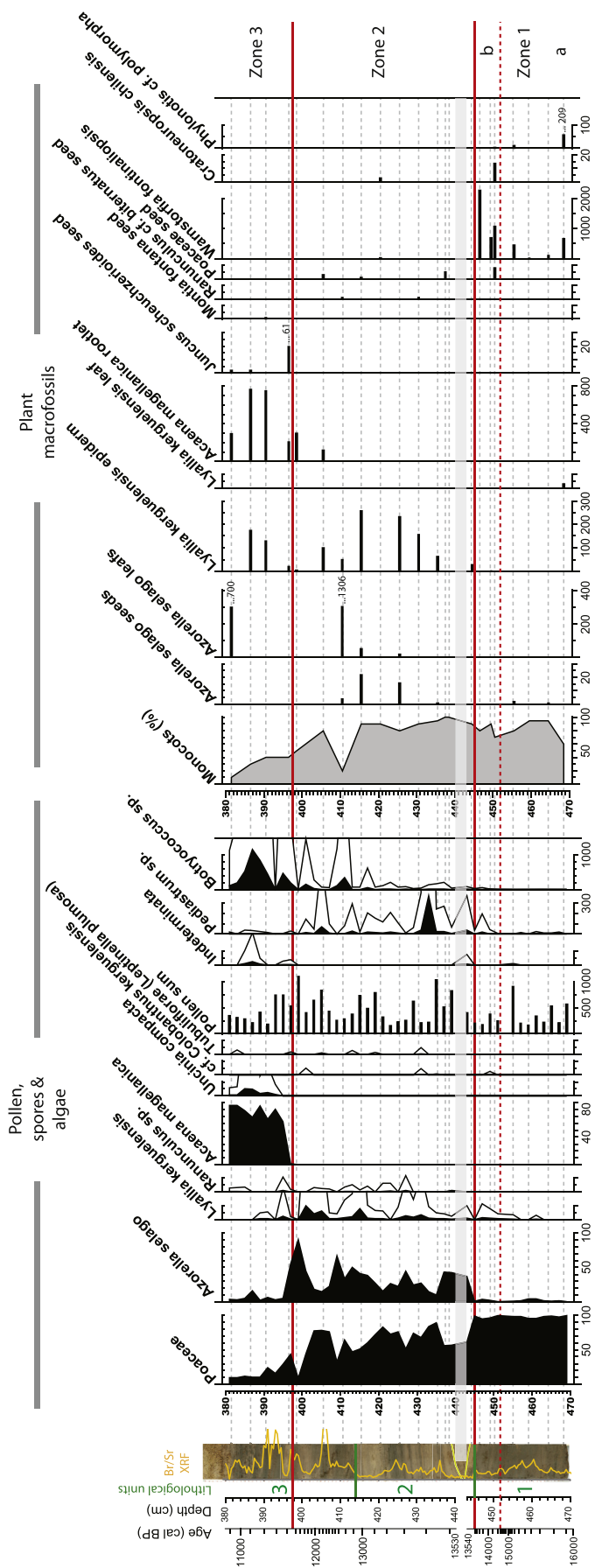


Fig. 4. Combined micro- and macrofossil diagram. Pollen data are expressed as percentages. Macrofossil data are expressed as concentrations except for Monocots, which are an estimate in % of the amount of Monocots in each sample. Dashed lines show the depths of the macrofossil samples.

incoherent and coherent (inc + coh) scattering to account for changes in the water content, density and grain size of the deposits during analysis (Kylander et al., 2012). Principal component analysis (PCA) was applied to the XRF data. Data were standardized prior to analysis using the equation  $z = (x - \mu)/\sigma$  in which  $\mu$  is the mean and  $\sigma$  the standard deviation of the series (e.g. Boyle, 2001). PCA was performed using the PAST program (Hammer et al., 2001).

### 3.3. Radiocarbon dating

Twenty samples for radiocarbon dating were submitted. Nineteen were sampled in the PVC tubes and one was sampled in the gouge auger sequence. Terrestrial plant remains such as *Azorella selago* leaves/seeds and mosses were picked whenever possible. However, in case of too little monospecific plant remains, a mix, and often containing monocot epidermis, had to be picked. One bulk sample was submitted. Samples were pre-treated by routine acid alkali acid (AAA) method. The  $^{14}\text{C}$  measurements were performed at the Single Stage AMS at Lund University (Sweden, LuS-samples) and at LMC14 (CEA Saclay, France, SacA-samples). An age–depth model was constructed in the calibration program OxCal 4.2 (Bronk Ramsey, 2009) applying the P-Sequence depositional model (Bronk Ramsey, 2008) and the ShCal 13  $^{14}\text{C}$  calibration curve (Hogg et al., 2013). A variable k-value was used as variations in accumulation rates were unknown (Bronk Ramsey and Lee, 2013). One date (LuS 10260) was excluded from the age–depth modelling as it was about 800  $^{14}\text{C}$  years too young.

### 3.4. Characterization of the organic matter: Rock-Eval6, peat humification and biogenic silica

A total of 41 levels (slices of 1 cm thick) for Rock-Eval6 analysis were sampled every 2–3 cm. Samples were dried overnight in an oven at 40 °C and then pulverized. The samples had a dry weight between 0.7 and 1.4 g. The pyrolysis program starts with an isothermal stage of 2 min at 200 °C. Then, the pyrolysis oven temperature was raised at 30 °C/min to 650 °C, and held for 3 min at this temperature. The oxidation phase, performed in a second oven under an air stream, starts at an isothermal stage at 400 °C, followed by an increase to 850 °C at 30 °C/min and kept at final temperature for 5 min (Jacob et al., 2004). Rock-Eval parameters are described by Espitalié et al. (1977) and specific parameters provided by the new RE6 by Lafargue et al. (1998).

The same number of samples, taken at the same sample depths as for Rock-Eval6 analysis, was used to determine the humification degree of the deposits using the colorimetric method as described in Chambers et al. (2010/11). Samples of 0.2 g of dried and grinded deposits were heated to c. 95 °C in an 8% NaOH solution for 1 h. Subsequently, the solution was well shaken and filtered using Whatman no. 1 filter papers. Three subsamples (after dilution with an equal volume of deionized water) of the solution of each sample were pipetted into cuvettes and measured with a spectrophotometer at 540 nm. Absorbance and % light transmission (%T) were recorded and an average of the three readings has been used in the calculation of % Absorbance (%A = 100 – %T). The %T and inconsequence %A of NaOH peat extracts can be used as a measure of peat decomposition (e.g. Caseldine et al., 2000). This method is mostly

used in raised, ombrotrophic peat bog deposits, in which one would expect that the deposits are build up by more or less pure organic matter. In the case of the Estacade sequence, OM is influenced by e.g. minerogenic matter input, “diluting” the OM signal. Therefore, we corrected the %A for the OM by calculating the %A/%TOC ratio (Roos-Barraclough et al., 2004).

Biogenic silica (BSi) analysis was performed on the same 41 levels as before, except for an additional sample at 393 cm and the 440 and 443 cm depths were replaced by samples at a depth of 439 and 443.5 cm, respectively. A wet-alkaline digestion technique described by Conley and Schelske (2001) was used. The samples were freeze-dried and grinded prior to analysis. Approximately 30 mg of sample was digested in 40 ml of a weak base (0.1 M Na<sub>2</sub>CO<sub>3</sub>) at 85 °C for a total duration of 5 h. Subsamples of 1 ml were removed after 3, 4 and 5 h and neutralized with 9 ml of 0.021 M HCl. Dissolved Si was then measured by the automated Molybdate Bleu Method (Grasshoff et al., 1983). During measurement it became clear that the amount of dissolved Si was high in most samples. High dissolved Si concentration indicated a negligible contribution of mineral fractions and therefore the mean of the three subsamples (3, 4 and 5 h) were retained as the amount of BSi (Conley and Schelske, 2001 but see also Clymans et al., 2015).

### 3.5. Palaeobotanical methods: pollen and plant macrofossils

Sampling for pollen analysis was done at every 2 cm, resulting in 44 samples (of c. 1 cm<sup>3</sup>) in total. The samples were processed using standard pollen extraction techniques (Faegri et al., 1989) based on gravity separation. For determination of the pollen types the studies of Barrow (1976) and Bellair (1967) were used together with a reference collection. The number of pollen grains found in the slides varies considerably from a minimum of 156 to a maximum of 1039, with a mean value of 441 grains. The pollen sum is defined as the sum of all native phanerogam taxa (see Van der Putten et al., 2010, online Supporting information, for a list of the native phanerogam species). The percentage diagram is constructed with Tilia Version 1.7.16 (Grimm, 2004).

Twenty-two samples (slices with a thickness of 1 cm and a volume between 4 and 14 cm<sup>3</sup>) were counted for their plant macrofossil content. Samples were taken at a range of levels. The samples were soaked overnight in a 5% NaOH solution and consequently washed gently through a 150 µm mesh sieve. After sieving, plant macrofossils were stored in a known volume of water (e.g. 200 ml). In this way, if in a given sample one or more taxa were dominant, a subsample of a known volume could be taken (after

stirring) in order to quantify this species (Janssens, 1983; Van der Putten et al., 2004). The sample material was systematically examined at 15 to 40× magnification using a stereomicroscope. Seeds, fruits, leaves and fragments of mosses were picked out and counted. For all samples, the absolute number of each species of seed, fruit or moss was calibrated for a standard sample volume. The proportion of monocot remains was estimated. The diagram is constructed with Tilia Version 1.7.16 (Grimm, 2004).

To summarize the pollen data, Principal Component Analysis (PCA) has been applied. The percentages were log-transformed (log(x + 1)), giving more weight to species which occur in lower abundances. PCA was performed using the PAST program (Hammer et al., 2001).

## 4. Results

### 4.1. Fieldwork

A coastal peat bank borders the eastern and northern coast line of the Péninsule Courbet (Fig. 1B), forming a relatively steep “cliff” facing the sea. The peat bank starts to occur from Pointe Charlotte and continues up to the north, to Cap Cotter and is only interrupted by the Rivière des Manchots and the Lac Marville (Fig. 1B). The thickness of the peat deposits ranges from 4 to 5 m in the south to c. 10 m in the north near Cap Cotter (Aubert de la Rüe, 1962 and personal observation by the first two authors). An asymmetric LGM ice cover was suggested by Hall (1984), centred over the west of the archipelago, so that the Péninsule Courbet may have been close to the eastern margin of the ice. The Estacade peat sequence has been sampled in the east of Péninsule Courbet (Fig. 1B) on top of the peat bank, just north of the hut (Cabane l'Estacade, Fig. 1C). Picture 1 (Fig. 1C) was taken at the foot of the peat bank, looking to the south, showing the hut with behind the “cliff”. Picture 2 (Fig. 1C) shows the coring site, looking in northern direction. The peat surface is rather flat and, about 300–400 m inland from the coast, e.g. 200–300 m inland from the coring site, the peat deposits fade and glacial sediments are exposed. Closed shallow ponds are present on these glacial sediments sometimes underlain by thin organic deposits (Figs. 1C and 5A). The area of Estacade is not influenced by fluvial activity. Important fluvial systems occur to the south of the site (Rivière du Bungay) and to the north (Rivière des Manchots) (Fig. 1B and C). These are also the areas where the coastal peat bank is absent.

It seems that peat accumulation was only possible on a restricted area of the Péninsule Courbet, as we know it today, as further inward no extensive peat deposits occur. However, at times



**Fig. 5.** Examples of peat ponds, i.e. shallow water bodies present on the peat surface in Kerguelen Islands today. (A) Shallow peat pond on the Péninsule Courbet (photo N. Van der Putten, December 2006), formed on relatively thin peat deposits, surrounded by *Acaena magellanica*. The bright green vegetation consists of *Ranunculus biternatus*. (B) Deeper peat pond (c. 40–50 cm water depth) in the broad valley of Plaine de Dante. The surrounding vegetation consists of Bryophytes and *Juncus* spp. together with some *Acaena magellanica*. Peat thickness is about 2 m (photo N. Van der Putten, December 2013). (For interpretation of the references to colour in this figure legend, the reader is referred to the web version of this article.)

**Table 1**  
Lithological description of the deposits between 470 and 381 cm depth at Estacade.

Unit	Depth (cm)	Description
3	470–445	Dark brown very compact slightly fibrous peat becoming more amorphous with some light brown very thin laminations from 452 cm onwards
2	445–414	Complex of light brown organic silty clay layers, with alternating darker brown more organic (peaty?) layers
1	414–381	Brown amorphous peat with alternating light brown layers. A light brown more silty to clayey sub layer is present at 397–395 cm. Presence of <i>Acaena magellanica</i> stems from 391 cm onward

of lower sea level, peat deposits may have extended beyond the current coastline. When sea level subsequently rose, peat deposits might have been eroded away. The interplay between eustatic and

local sea level changes, however, is poorly constrained on Kerguelen Islands (Hodgson et al., 2014 and references there in). During fieldwork, it was observed that in front of the peat bank big

**Table 2**  
Radiocarbon dated samples from the lower part of the Estacade sequence, displaying sample depth,  $^{14}\text{C}$  age, calibrated age and type of material dated. The omitted date in the age–depth model is shown in italic. The sample below the dashed line is the basal sample of the gauge sequence.

Code	Depth below surface (cm)	$^{14}\text{C}$ age (yr BP)	Calibrated ages (median)	Calibrated ages $2\sigma$ age ranges	Material dated
LuS 9407	381.5	9690 ± 65	10901	2σ 11142–10756	<i>Azorella selago</i> leaves
SacA 35759	384.5	9740 ± 45	11032	2σ 11187–10820	<i>A. magellanica</i> twigs
LuS 10257	387.5	9655 ± 60	11117	2σ 11204–10911	<i>A. magellanica</i> twigs/roots
SacA 35760	393.5	9950 ± 60	11301	2σ 11474–11204	Higher plant epidermis
LuS 9890	398.5	9945 ± 65	11492	2σ 11707–11273	<i>A. magellanica</i> rootlets
LuS 10258	405.5	10355 ± 75	12180	2σ 12424–11840	Higher plant epidermis + <i>A. magellanica</i> twigs/roots
LuS 9408	410.5	10910 ± 65	12746	2σ 12858–12676	<i>Azorella selago</i> leaves
LuS 10259	415.5	11125 ± 70	12981	2σ 13095–12816	<i>A. selago</i> seeds
LuS 9891	423.5	11510 ± 70	13238	2σ 13365–13118	<i>A. selago</i> leaves
SacA 24097	435.5	11660 ± 60	13447	2σ 13547–13356	Higher plant epidermis
SacA 35761	438.25	11680 ± 70	13495	2σ 13583–13406	Higher plant epidermis
<i>LuS 10260</i>	<i>441.5</i>	<i>10880 ± 75</i>	<i>12736</i>	<i>2σ 12913–12652</i>	<i>A. selago</i> seeds
LuS 10605	444.5	11765 ± 70	13555	2σ 13717–13456	Higher plant epidermis
LuS 9409	446.5	12090 ± 75	13853	2σ 14090–13711	Higher plant epidermis
LuS 10261	451.5	12255 ± 75	14238	2σ 14710–13975	Higher plant epidermis + moss leaves
LuS 11078	452	12580 ± 60	14716	2σ 15079–14277	Higher plant epidermis + moss leaves
LuS 9892	455.5	12940 ± 75	15332	2σ 15582–15128	Higher plant epidermis
LuS 10262	460.5	13230 ± 85	15657	2σ 15863–15395	Higher plant epidermis
SacA 7753	468.5	13190 ± 50	15877	2σ 16057–15689	Bulk peat
SacA 24098		13240 ± 60			Higher plant epidermis + moss leaves

rounded pebbles were present, probably representing an ancient beach level. The altitude of this ancient beach is about 2–3 m asl, suggesting a restricted post-glacial isostatic rebound. One could imagine that at least part of the peat deposits was cut by sea erosion during the time that this beach was active. Interesting is that the peat bank kept on accumulating and still accumulates today. We want to stress that the term “peat bank” here only refers to its morphological aspect (a “cliff”) and should not be confused with moss peat banks as known from the Antarctic Peninsula and South Georgia (Van der Putten et al., 2009), a semi-ombrotrophic peat bog dominated by two moss species (*Polytrichum strictum* and *Chorisodontium aciphyllum*). Such moss peat banks do not occur on Kerguelen Islands. The vegetation on the Estacade site today is largely dominated by *Acaena magellanica* (Fig. 1C, picture 2). However, the peat bank bordering the coast line of the Péninsule Courbet is considered to have been fed chiefly by atmospheric deposition right after its formation, with limited contribution of seepage water.

#### 4.2. Stratigraphy

In Fig. 2, a sediment log is shown with a depth scale and the lithological units are described in Table 1. As is seen on the core log, laminations are not always horizontal. Therefore, we used the middle of the core to determine the depths of the boundaries reported in Table 1. A yellow–light brown layer, forming a triangle (shown by the yellow lines in the log in Figs. 2 and 4), is present between 443 and 440 cm. It contains coarse minerogenic grains. Thin layers of coarse sand (c. 0.5 cm thick) are found at 391.5, 431.5 and 445 cm.

#### 4.3. Radiocarbon dating

All necessary information regarding the radiocarbon dated levels for the age–depth model is shown in Table 2. One date (441.5 cm) has been omitted from the age model as it was about 800 <sup>14</sup>C years too young in comparison with the dates just above and below. The sample was taken in the coarse grained triangle (see yellow (in the web version) lines in the log in Figs. 2 and 4). The basal age of the gouge auger sequence is identical, within uncertainties, to the basal age of the sequence sampled in the CALYPSO tube (Table 2) indicating that the onset of peat accumulation is captured in the CALYPSO tube. The age–depth model based on the median values together with the 2σ errors and the accumulation rates (mm/yr) are shown on Fig. 2. An age–scale is added on both Figs. 2 and 4.

#### 4.4. Rockmagnetic, geochemical analyses and characterization of the organic matter: Rock-Eval6, peat humification and biogenic silica

In Fig. 2 the following selected data are shown: magnetic susceptibility (MS) plotted with the Ca/Br and Ti/Br ratios; the K/Ti ratio, Axis 2 of the PCA analysis on the XRF data set; biogenic silica (BSi); total organic carbon (TOC) plotted with Br/Sr; hydrogen index (HI), oxygen index (OI) and the HI/OI ratio (Rock-Eval6); and the % Absorbance/% TOC ratio. We have divided the whole data set in three divisions (1–3), each divided in two sub-divisions (a, b).

##### 4.4.1. Minerogenic proxies

In general, MS is variable throughout the sequence except in division 1 (470–445 cm), where MS values fluctuate between 20 and 40 · 10<sup>-6</sup> SI. A sudden increase occurs at the onset of division 2 and values stay high until 437 cm after which MS values vary between -1.5 and 40 · 10<sup>-6</sup> SI. MS, Ca/Br and Ti/Br ratios are

assumed to be related to the minerogenic content of the deposits; the trends are very similar although fluctuations in the Ca/Br and Ti/Br curves are more pronounced in division 2a. In the scatterplot (Fig. 3) of the PCA the first axis (PC1) explains 49% of the variance and clearly discriminates Br from all the other elements. The second axis (PC2, Figs. 2 and 3) explains 28% of the variance and differentiates between two groups of elements: group 1 (positive values) are elements such as Fe, Ti, Sr and Ca and group 2 (negative values) are e.g. K and Rb. The three divisions are reflected in axis 2 (Fig. 2): division 1 shows the most positive values suggesting that group 1 elements are dominating; division 2 shows values fluctuating around 0 and in consequence group 1 elements are less prominent in comparison with division 1; division 3, based on the negative values, is characterized by group 2 elements.

##### 4.4.2. Organic matter proxies

Several sources exist for BSi (e.g. Sommer et al., 2006). In the Estacade sequence, BSi mainly originates from diatoms as was observed in smear slides from the different divisions and in SEM images (Supplementary Material). BSi values vary, but are relatively high throughout the sequence. In division 1, BSi gradually increases from 2% at 468 cm to a maximum of 13% at 448 cm depth. Division 2 is characterized by high amounts of BSi, up to a maximum of nearly 25% (433 cm). Values decrease drastically at the onset of division 3a and become slightly higher again in division 3b.

The Rock-Eval parameters represented in this study are the following: (i) Total Organic Carbon (TOC, %); (ii) Hydrogen Index (HI, in mg HC/g TOC) and (iii) Oxygen Index OIR6 (in mg O<sub>2</sub>/g TOC).

TOC values represent the total amount of organic matter (OM) in the sediment sample. In general, the TOC curve is anti-correlated to the MS, Ca/Br and Ti/Br curves. TOC values are higher than 20% in division 1a (c. 25%), in parts of division 2b (c. 24%), in division 3a (c. 38% except for the sample at 396 cm) and the top two samples of division 3b. The lowest TOC values are found in division 2a, ranging from c. 6–20%. From the PCA analysis on the XRF data it is clear that Br behaves differently compared to all other elements. We have plotted the Br/Sr ratio with the TOC curve, and the correlation between the curves is striking for all divisions, and somewhat less for division 1a. The Br/Sr ratios in Figs. 2 and 4 correlate well with the coloured stratigraphic log. Darker, more organic parts, show higher values for Br/Sr.

The Hydrogen Index (HI) is the amount of hydrocarbonaceous (HC) products released during pyrolysis normalized to TOC. HI values of 250–350 mg HC/g TOC are typical of well-preserved higher plant OM (Jacob et al., 2004). In the Estacade sequence, however, most values are higher than 350 mg HC/g TOC suggesting different sources (terrestrial + aquatic) of organic matter except in division 1 and 3b. HI values higher than 500 mg HC/g TOC indicate the notable presence of algae (sample at 433 cm and in zone 3a).

The Oxygen Index Rock-Eval 6 (OIR6) is an estimate for the oxygen content of the OM. OIR6 varies between 90 and 237 mg O<sub>2</sub>/g TOC. Mostly, values vary around 120 O<sub>2</sub>/g TOC except in division 1a and 3b where values are higher.

Opposite trends in the HI and OIR6 curves are also used as an indicator for the degree of preservation of the OM (e.g. high HI and low OIR6 point to a good preservation of the OM). Here we calculated the ratio between the HI and OI. High HI/OI ratios reflect low humification or a good preservation of the OM, and *vice versa*. Humification is higher in divisions 1 and 3b.

Furthermore, we measured the humification of the OM using the colorimetric method which results in an independent record of OM preservation that can be compared with the results of the HI/OI ratio from the Rock-Eval6 analyses. The two humification records show similar patterns.

In general, division 1 and 3 are, based on the lithology, consist of peat deposits although a certain degree of aquatic OM is present (especially in division 3a). However, we interpret the HI/OI ratio in these divisions as reflecting the preservation of the OM rather than the origin of OM (Disnar et al., 2003). In division 2, showing relatively high values for the HI index, well preserved aquatic OM is present and here the HI/OI ratio represents both the origin of OM as well as the preservation of it.

#### 4.5. Palaeobotanical results: pollen and plant macrofossils

Fig. 4 shows a combined microfossil-macrofossil diagram. The zonation of the diagram is based on the pollen and macrofossil data.

Zone 1 (470–445 cm) is dominated by Poaceae. *A. selago* is also present in zone 1 and *Lyallia kerguelensis* starts to occur from 455 cm and upwards but the number of grains found is low. The dominance of Poaceae in the pollen spectra is confirmed by the high percentage of Monocots in the macrofossil diagram. Furthermore, zone 1 is characterized by the presence of the moss species *Warnstorfia fontinaliopsis* and to a lesser extent by *Cratoneurospis chilensis* and *Phylonotis* cf. *polymorpha*. Zone 1b shows higher numbers of *W. fontinaliopsis* than in zone 1a. *Pediastrum* sp. (green algae) starts to become more important in Zone 1b.

In Zone 2 (445–397 cm), *A. selago* and *L. kerguelensis* occur in considerable numbers, together with *Pediastrum* sp. and a second algae, *Botryococcus* sp. *Ranunculus* sp. pollen grains are found from 427 and upwards. Seeds of the same species are very few but both were found in zone 2. Macrofossils from *L. kerguelensis* are present throughout zone 2 in contrast to *A. selago*, which occurs more sporadic, and not in every sample. It is noteworthy that the sample at 420.5 cm contains no remains of the latter species, while this sample is the only one outside zone 1 in which moss remains were found.

Zone 3 (397–380 cm) is characterized by the sudden expansion of *A. magellanica* both in the pollen and the macrofossil data set. However, *A. magellanica* macro remains already start to occur in the top samples of zone 2, as they consist of rootlets of the plant. *Juncus scheuchzeroides* seeds are only present in zone 3, and in the pollen diagram *Uncinia compacta* expands slightly later than *A. magellanica*. *Pediastrum* sp. nearly disappears and *Botryococcus* sp. seems to take over and shows its highest percentages in this zone. Both *A. selago* and *L. kerguelensis* are still present in the pollen record of zone 3, but in much lower quantities than before. In contrast, in the first half of the zone *L. kerguelensis* macrofossils are still abundant. In the top sample (381.5 cm), a high number of *A. selago* leaves was found, while in the pollen record *A. selago* plays a minor role. In general, micro- and macrofossil data coincide rather well throughout the Estacade sequence.

Pollen data are summarized as the second axis of a PCA. The first axis (PC1, 55% of variance) discriminates between Poaceae and all

other species included in the PCA. The second axis (PC2, 28% of variance) rather discriminates between *A. magellanica* and *A. selago*.

## 5. Discussion

### 5.1. Stratigraphy and age-model

Based on a radiocarbon date at a depth of 441.5 cm ( $10,880 \pm 75$   $^{14}\text{C}$  yr BP, Table 2) and the stratigraphy of the record (yellow (in the web version) triangle in core log in Figs. 2 and 4), it became clear that a c. 800 year younger layer is intercalated. A grey band is plotted on both Figs. 2 and 4 to indicate the layer. It is usually difficult to explain younger intercalated deposits in what seems to be an otherwise normally accumulating sequence. The sample submitted for dating consisted of *A. selago* seeds. These seeds are not present in the samples at 444.5 and 438.25 cm depth, just above and below the intercalated layer. However, *A. selago* macrofossils start to occur at a depth of 425 cm. A likely hypothesis is that channels/gullies started to form and cut through the deposits about 12,750 cal yr BP. Incision stopped on the more compact peat of zone 1. We cannot exclude a short erosional hiatus, but based on the radiocarbon dates of the layers below and above the intercalation it is of short duration. Peat channels, sometimes in connection with sink holes, are common in the mires of Kerguelen Islands today.

### 5.2. Proxy interpretation

In Table 3 we summarise the different proxies used in this study together with their interpretation. The palaeobotanical data (pollen and macrofossils), BSi, MS, TOC together with the lithology are the main proxies on which the palaeoenvironmental reconstruction of the Estacade site is based. We are aware of the fact that XRF core scanning data are not quantitative and thus do not represent elemental concentration data. However, we use the relative changes in the elemental composition of the deposits to corroborate the reconstruction of past environmental changes based on other independently measured proxies.

From the PCA analysis of the XRF data (Fig. 3), it became clear that Br shows a different pattern compared to all other elements. Br is mainly of marine origin and Br measured by XRF core scanning has been regarded as a proxy for atmospheric deposition of sea-salt aerosols (and in consequence for wind intensity) in peat deposits, especially for sites that are situated close to the sea (Unkel et al., 2010). However, in the Estacade record, Br seems to relate closely to the amount of organic matter as expressed by the Br/Sr ratio. The use of Br concentrations in peat deposits as reflecting true atmospheric deposition rates has been discussed (Shotyky, 1997; Biester et al., 2004). Biester et al. (2004) conclude from their study of two Chilean peat bogs that Br in peat exists in an organically bound form and that the element is not conservative in bogs. Hence, peat

**Table 3**

A list of the proxies used in this study and how they are interpreted. Note that all interpretations are qualitative.

Proxy	Description	Interpretation
Plant micro- and macrofossils	Proxy for past regional and local vegetation changes	Wind strength, humidity, relative temperature
BSi	Proxy for diatom productivity	Terrestrial vs. pond/lake
TOC	Proxy for OM content	Terrestrial vs. pond/lake
HI/OI	Proxy for the preservation of the OM and/or origin of the OM	Humidity/relative temperature
%Abs/%TOC	Proxy for the preservation of the OM	Humidity/relative temperature
Br/Sr	Proxy for OM content (high resolution)	Terrestrial vs. pond/lake
Ca/Br & Ti/Br	Proxy for minerogenic content (high resolution)	Wind strength
MS	Proxy for minerogenic content (high resolution)	Wind strength

decomposition has a significant influence on Br concentrations in peat deposits. In consequence, we will not consider Br as a sea-salt/wind proxy in our study but rather as a proxy for amount of OM.

The second axis of PCA applied to the XRF data resulted in the division of two groups of elements (Figs. 2 and 3): group 1 with Fe, Ti, Sr and Ca and group 2 with K and Rb. Group 1 elements might originate from the erosion and weathering of the basaltic rocks (e.g. olivine, pyroxenes) that dominate the geology of Kerguelen Islands while group 2 is probably more characteristic for a potassic ash. Often the presence of Ca is related to within “lake” formation/deposition of organic CaCO<sub>3</sub> (e.g. Johnson et al., 2011; Liu et al., 2013). However, in a geological setting dominated of basaltic lava flows, carbonate deposition is unlikely. SEM images at 413, 430 and 440 cm depth reveal that the samples are dominated by diatom frustules and fine grained minerogenic material (Supplementary data). Moreover, the Ca/Br and Ti/Br curves show a similar pattern (Fig. 2) and in consequence we conclude that Ca is not originating from precipitation of carbonates but from an external minerogenic source. Beside the main elements SiO<sub>2</sub> (~45–50 wt%), Al<sub>2</sub>O<sub>3</sub> (~13–18 wt%) and Fe-oxydes (~10–14 wt%), CaO (~10 wt%) and TiO<sub>2</sub> (~3 wt%) are important elements in basaltic rocks originating from the Kerguelen archipelago (Gautier et al., 1990). Within the trace elements Sr is the most abundant one (Gautier et al., 1990). In consequence we regard group 1 as representative for basaltic rocks. Group 2 is characterised by K and Rb. Tephra originating from Kerguelen can be classified as trachytes and show a chemical composition with high amounts of SiO<sub>2</sub> (~64.6 wt%), Al<sub>2</sub>O<sub>3</sub> (~15.9 wt%), Fe-oxydes (~5.6 wt%), Na<sub>2</sub>O (~6.4 wt%) and K<sub>2</sub>O (~4.9 wt%). TiO<sub>2</sub> (~0.4 wt%) and CaO (~0.9 wt%) are present but in lower amounts in comparison with basaltic lavas. We conclude that group 2 is representative for a potassic ash and the K/Ti ratio can be used as a proxy for the relative presence of tephra in our record (Fig. 2). In conclusion, PCA axis 2 discriminates between two different sources for the minerogenic content of the Estacade record, a potassic ash on the one hand and weathering products of basaltic lavas on the other.

XRF Core scanning elemental ratios such as Si/Ti have been used to estimate the amount of BSi in several studies (e.g. Johnson et al., 2011; Liu et al., 2013). However, in the case of our record, Si sources are multiple: basalts, potassic ash and biogenic. The XRF derived Si incorporates all these sources and therefore the former ratio does not reflect BSi and is not used in our study.

The morphological setting of the peat bank (semi-ombrotrophic), the absence of fluvial activity in the Estacade area, the lithology (peat and very fine grained sediments, clays) together with the overall robust age–depth model of the sequence suggests that the site was not largely affected by runoff and in consequence we consider minerogenic particles to be windborne rather than waterborne.

The onset of peat growth at about 16,000 cal yr BP can be regarded as a minimum age of deglaciation of the Estacade site. Peat accumulation continued until 13,600 cal yr BP and was characterized by the presence of *W. fontinaliopsis*, a moss species growing in wet conditions on mires (Fig. 4). Also Poaceae (monocots in macro fossil diagram) were abundantly present. TOC is relatively high (c. 20%) and the amount of minerogenic content is low (Fig. 2). OM is generally well preserved. However, accumulation rates are highly variable between 16,000 and 13,600 cal yr BP. Around 14,800 cal yr BP accumulation rates decrease drastically. This could suggest a hiatus but visual inspection of the core does not show any evidence of an erosional discordance. We suggest that the conditions (relatively warm and dry) were such that peat was highly humified at the end of zone 1a, resulting in decreased accumulation rates. At the onset of zone 1b (452 cm), a change to more humid conditions occurred: *W. fontinaliopsis* thrives, BSi

values are high suggesting diatom blooms and *Pediastrum* sp. becomes more important. TOC decreases slightly in comparison with zone 1a, probably because of a dilution effect by slightly increased minerogenic content (Ca/Br and Ti/Br curves), increased BSi together with higher accumulation rates. The OM is, however, better preserved than in zone 1a, as a result of a higher water table in the mire. The onset of these wetter conditions dates to about 14,550 cal yr BP, but the errors in the age model at this depth are very large (2σ ranges cover 960 years).

About 13,600 cal yr BP, a sudden shift in all proxy data occurs. A change from peat to organic silty clay deposits can be observed in the core log in Figs. 2 and 4. Accumulation rates increase drastically probably as a consequence of a higher input of minerogenic material (MS, Ca/Br and Ti/Br curves, Fig. 2). As a result TOC decreases but the OM matter is well preserved (%A/%TOC and HI/OI). A higher HI index suggests the presence of aquatic OM. Accumulation rates stay high until 12,920 cal yr BP, corresponding to division 2a. A sudden expansion of the plant species *A. selago* can be seen in the pollen data. *L. kerguelensis*, although already present in zone 1, becomes more important in zone 2, together with *Pediastrum* sp. and *Botryococcus* sp. algae, indicating open water. From the macrofossil record it can be concluded that both *A. selago* and *L. kerguelensis* were growing on or close to the coring site. The darker more peaty parts present in the core log, also shown by the higher values in the Br/Sr ratio, coincide with higher TOC and findings of macrofossils of *A. selago* and *L. kerguelensis*. At the same time BSi (and to a lesser extent *Pediastrum* sp.) shows lower values in the peaty parts as well as the HI/OI ratio. Between 13,600 and 12,900 cal yr BP, we think the Estacade site was characterized by the presence of peat ponds, i.e. shallow water bodies, without inlet nor outlet, on the peat surface in which diatoms and algae could thrive and lacustrine-type sediments were deposited (Fig. 5). Today peat ponds are present on the Péninsule Courbet (Fig. 5A) and in most of the large valleys characterized by mires (e.g. Plaine de Dante, Fig. 5B).

Higher accumulation rates are, beside increased BSi production, probably the result of increased input of minerogenic material into the ponds, and wind is the most likely transport agent for the mineral matter in ponds surrounded by peat. Increased windiness can also be deduced from the presence of *A. selago* and *L. kerguelensis*, both cushion plants that are very well adapted to withstand extreme winds (Wagstaff and Hennion, 2007). Today these species, and especially *A. selago*, are found on the higher exposed plateaus in the archipelago, forming the so-called fell-field vegetation together with bryophytes (Van der Putten et al., 2012a). About 12,900 years ago, both pollen taxa are still present but macrofossil concentrations decrease. Minerogenic content (Ca/Br and Ti/Br, Fig. 2) drops suddenly and so does the accumulation rate. TOC increases and BSi percentages stay more or less at the same level. *Botryococcus* sp. becomes more important. The proxy data suggest less windy conditions after 12,900 cal yr BP revealed by the lower minerogenic content (Fig. 3, division 2a). However, *A. selago* and *L. kerguelensis* are still the main plant species. *Botryococcus* is often presented in microfossil diagrams but is rarely interpreted in a palaeoecological context. This alga is found in shallow and oxygenated freshwater lakes and ponds, bogs and puddles (Guy-Ohlson, 1992). Demetrescu (1999) states that “Well preserved colonial specimens always reflect settling in a protected depositional site with calm waters and minimal climatic variations. When a given factor (such as wind, for instance) disturbs the habitat equilibrium, the colonies sink and reach again the water surface only after the calm status is restored”. In consequence, the higher amount of this alga in the Estacade record from 12,900 cal yr BP and onward, could also point to less wind stress. In conclusion, between 12,900 and 11,500 cal yr BP the environment seems to be

characterized by, relatively speaking, less windy, drier and/or warmer conditions. It may be that the climatic conditions became more seasonal and that the ponds dried out during summers, resulting in a possible temporary colonisation by higher plants during summer and hence higher “terrestrial” OM.

The period between 11,500 and 10,900 cal yr BP is characterized by the sudden expansion of *A. magellanica*, in the pollen as well as in the macrofossil data. The rootlets of this species are already present c. 5 cm lower. Somewhat later, at about 11,350 cal yr BP *U. compacta* occurs for the first time in the Estacade record. Both species grow in sheltered habitats. Young and Schofield (1973) regarded these species as warm “lowland” species, while the occurrence of *A. selago* is evidence for cold “upland” conditions. In a comparison between pollen data and macrofossil data, Van der Putten et al. (2012b) concluded that such an “upland-lowland principle” is difficult to apply for sub-Antarctic palaeoclimatic interpretations, at least for the Holocene period. However, for the Last Termination with its more pronounced climatic changes, this principle seems to be valid based on the shift from an *Azorella* dominated period to an *Acaena* dominated period at 11,500 cal yr BP. In this context it is noteworthy that the onset of the occurrence of *Acaena* in Core 2 (Port Douzième, Presqu’île Ronarch, Fig. 1B) in Young and Schofield (1973), after calibration of their initial radiocarbon dates and interpolation between the dates, can be estimated to about 11,600 cal yr BP, coinciding with the onset in the Estacade record.

Based on the geophysical and geochemical data (Fig. 2), the period between 11,650 and 10,900 cal yr BP can be subdivided in two sub-periods (divisions 3a and b, Fig. 2). The onset of division 3a is characterized by a sudden drop in BSi, while TOC shows the highest values of the whole record. Accumulation rates increase, but here it seems not to be related to increased minerogenic input. The proxy data point to drier and more terrestrial conditions, but with good preservation of the organic matter and wet enough conditions for *Botryococcus* sp. to bloom. *Pediastrum* sp., however, nearly disappears suggesting that the peat pond milieu had ceased at that time. From 11,225 cal yr BP onwards TOC decreases. The preservation of the OM is rather bad as can be seen in both the HI/OI and the %Abs/%TOC ratios. BSi increases but values stay well below the values measured before 11,650 cal yr BP. It seems that a rather well oxidized peat was formed 11,225 cal yr BP, with still wet enough conditions for *Botryococcus* and diatoms to bloom. Interesting is, that from that time onward, cross sections of *Acaena* twigs can be seen in the core, which are not present before. Maybe *Acaena* started to grow around the site at the start of the Holocene (11,500 cal yr BP) due to warmer (drier) conditions but invaded the site itself somewhat later (11,225 cal yr BP). One can imagine that peat, formed by this woody dwarf shrub with a dense interlacing twig and root system, results in a more oxidized peat than *Azorella* peat.

The second axis of PCA applied to the XRF data discriminates between two groups of elements (Figs. 2 and 3): group 1 with Fe, Ti, Sr and Ca and group 2 with K and Rb. Group 1 elements might originate from the erosion and weathering of the basaltic rocks while group 2 is more characteristic for a potassic ash. Group 1 is very prominent between 16,000 and 13,600 cal yr BP and to a lesser extent also between 13,600 and 11,650 cal yr BP. From c. 11,650 cal yr BP, elements of group 2 become prominent (Fig. 2). The second axis, therefore, might reflect a change in source area of the minerogenic particles in our record. One could imagine that, during deglaciation of Kerguelen Islands, source areas for fine grained mineral particles, originating from erosion of basaltic bedrock, greatly expanded as a result of retreating glaciers. Although less minerogenic material is present before 13,600 cal yr BP it seems that it is dominated by the basaltic component (group 1). Between

13,600 and 11,650 cal yr BP, both components (basaltic and ash) add to the minerogenic content. From 11,650 cal yr BP onward, the elements referring to a potassic ash become more important. By then deglaciated areas were covered by vegetation, stabilizing soils and diminishing the source area for basaltic minerogenics, a process that probably already started earlier. The presence of tephra in peat deposits from the Kerguelen archipelago is not straightforward related to volcanic eruptions. Reworked ash deposits are abundant on the archipelago in some cases even forming dunes. One has to take into account that ash is transported by wind constantly and that it is sometimes difficult to distinguish between a “real” tephra layer, resulting from a volcanic eruption, and a tephra deposit resulting from the reworking of tephra related to older eruptions.

### 5.3. Palaeoenvironmental and climatic reconstruction

#### 5.3.1. Climatic reconstruction of Kerguelen Islands and comparison with the EDC ice core

In Fig. 6, we present selected proxy data of the Estacade record on an age scale and show the climatic interpretation of the data.

The onset of peat growth at the Estacade site 16,000 cal yr BP coincides with the post-LGM warming in Antarctica, which already started 18,350 cal yr BP (EPICA Dome C ice core, Veres et al., 2013). Both temperature and effective precipitation (precipitation – evapotranspiration) were high enough to allow plants to expand from their LGM-refugia (Van der Putten et al., 2010) and to provide the humid conditions for peat to form and be preserved. TOC is high and BSi gradually increases. Vegetation is dominated by Poaceae and the wet loving moss *W. fontinaliopsis*. We infer relatively warm, wet and stable conditions becoming slightly wetter about 14,550 cal yr BP. About 13,600 years ago a sudden change can be observed in our proxy-data. The peat gives way to a laminated lacustrine-type of deposit with alternating more minerogenic and more organic layers. *A. selago* and *L. kerguelensis*, cushion plants which today occur on wind swept plateaus in the archipelago, expand suddenly and become important plant species. The algae *Pediastrum* sp. occurs, followed closely by a sharp increase of BSi caused by diatom blooms suggesting open water conditions. Climate conditions became wetter, allowing small ponds to form on the peat surface, and windier, the latter resulting in higher amount of minerogenic material together with the expansion of the wind tolerant plant species. An intensification of the SHW could explain our proxy data from 13,600 ( $2\sigma$  13,765–13,450) cal yr BP onwards. Based on the pollen, BSi and *Pediastrum* curves, these wet and windy conditions continued until c. 11,600 cal yr BP. However, based on the drop in minerogenic content, higher TOC and high amounts of *Botryococcus* sp. it seems that conditions became less windy and less humid c. 12,900 cal yr BP. About 11,650 years ago, pond deposits were replaced by peat deposits and *A. magellanica* and *U. compacta* became the dominant plant species on the site, growing in sheltered and warmer conditions. Wet indicators (BSi and *Pediastrum*) become less prominent or disappear. Warm and dry climate conditions, less influenced by the SHW occurred on Kerguelen Islands after 11,600 cal yr BP, coinciding with the early Holocene climate optimum in the Antarctic ice records (Masson et al., 2000). Frenot et al. (1997) studied the sensitivity of the Ampère glacier of the Cook ice cap by mapping the glacier extent between 1962–1995 in relation to changes in temperature and precipitation. In an area rapidly deglaciated during the warm and relatively dry 1990s they found well-preserved peat deposits close to the retreating glacier snout which they dated to c. 11,800–11,300 cal yr BP, i.e. the Pleistocene–Holocene transition. It implies that the glacier front at least retreated to the 1995 position during the warm and drier conditions of the early Holocene in the Estacade record.

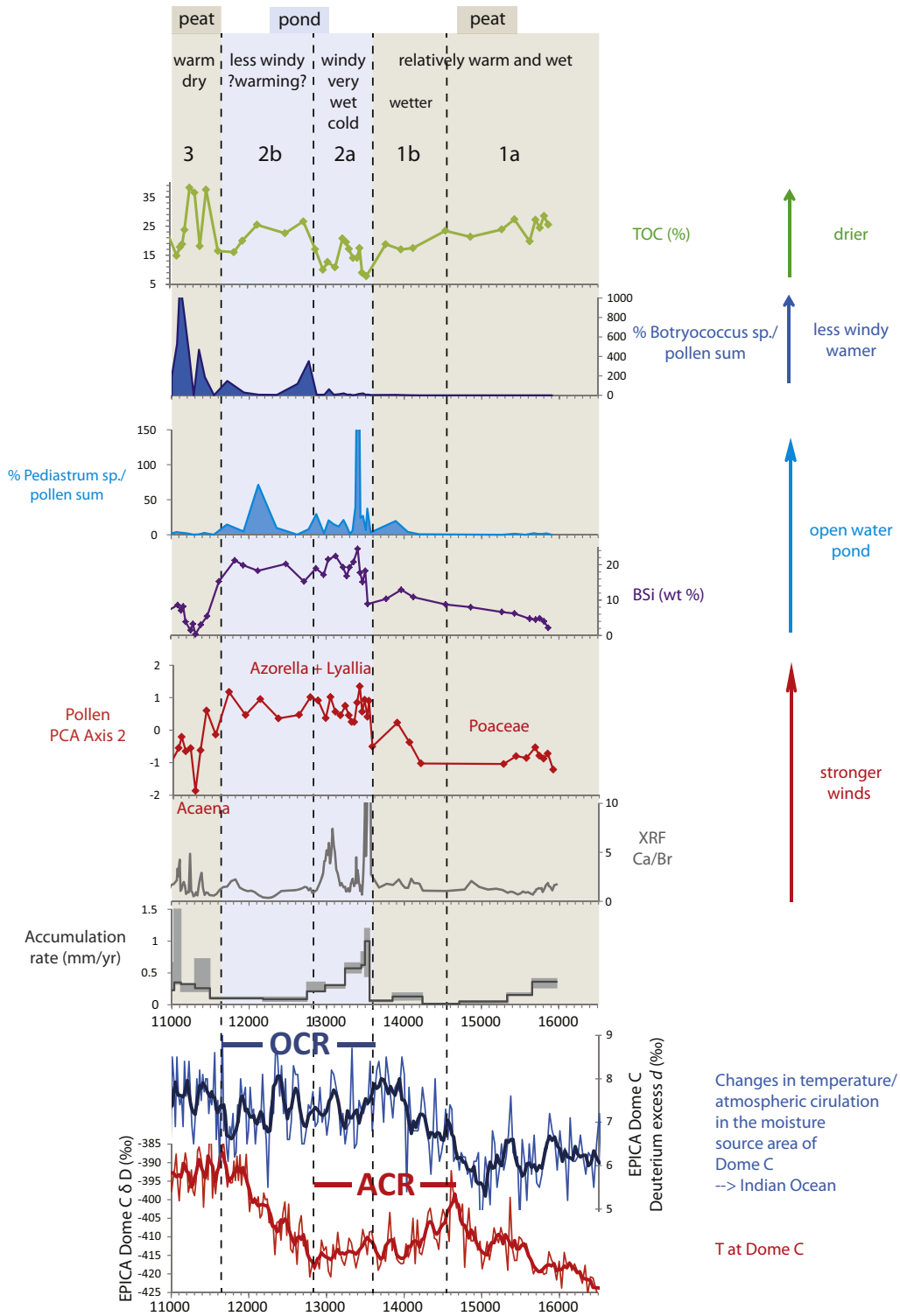


**Fig. 6.** Selected proxy data from the Estacade peat record on an age scale compared to the  $\delta D$  and deuterium excess  $d$  record of the EPICA Dome C ice core on the chronology proposed by Veres et al. (2013).

We plotted  $\delta D$  and deuterium excess  $d$  (Fig. 6) of the EPICA Dome C ice core record on the chronology proposed by Veres et al. (2013).  $\delta D$  reflects surface temperature changes at the Dome C site while  $d$  was interpreted to represent the sea surface temperature (SST) in the moisture source area (Stenni et al., 2001). The main moisture source of Dome C is the southern Indian Ocean (stippled area in Fig. 1A). Stenni et al. (2001) inferred

that an Oceanic Cold Reversal (OCR) took place in the south Indian Ocean, c. 1000 years after the onset of the Antarctic Cold Reversal (ACR), at c. 13,650 ( $1\sigma$  13,190–14,110) cal yr BP and 14,650 ( $1\sigma$  14,190–15,110) cal yr BP, respectively, based on the new chronology (Veres et al., 2013). If we compare our proxy-data from the terrestrial/atmospheric record from Kerguelen Islands with the data from EDC, the occurrence of an OCR in the

moisture source area of Dome C seems to be confirmed. Stenni et al. (2001) concluded that the meridional temperature gradient between Dome C and its source area was the largest at the onset of the OCR (13,650 cal yr BP) causing a possible intensification of the mid- and high latitude atmospheric circulation, e.g. intensification of the SHW, which is supported by our data (Fig. 6). However, interpretation of deuterium excess  $d$  is not straightforward. Whether it reflects SST changes or a shift in the moisture source area is still not clear (Stenni et al., 2010). Also, comparison of  $d$  data between the East Antarctic EDML (EPICA Dronning Maud Land) and EDC ice cores, with source areas in the south Atlantic and south Indian Ocean, respectively, revealed different trends of moisture source temperatures (Stenni et al., 2011). These different shifts in moisture sources are probably related to reorganization of atmospheric circulation at ocean basin scale, suggesting a different expression of the bipolar seesaw in the two basins (Stenni et al., 2011). Our proxy data show no clear change at the onset of the ACR. However, based on our proxies it is not possible to reconstruct temperature changes in a quantitative way. If the ACR is mainly a shift to colder conditions without a significant change in atmospheric circulation, as could be the case based on the deuterium excess  $d$  data from the EDC ice core, it is probable that the ACR is not registered in our proxy data. Nevertheless, one could speculate that the onset of the slightly wetter conditions c. 14,550 cal yr BP ( $2\sigma$  15,020–14,061), taking into account the large uncertainties in the age–depth model at that time, is caused by colder conditions at the onset of the ACR.

### 5.3.2. The Kerguelen Islands data set in a larger SHW context

Toggweiler et al., 2006, suggested that during the LGM, atmospheric  $\text{CO}_2$  was lower due to reduced exchange between the deep ocean and the atmosphere through the Southern Ocean. This reduced upwelling at the Antarctic Divergence would be the result of an equator-ward position of the SHW. For cold periods in the Northern Hemisphere (coinciding with warming in the South) during the Last Termination, such as Heinrich Stadial 1 (HS1) and YD, a southward shift of the ITCZ and the SHW has been proposed resulting in increased  $\text{CO}_2$  ventilation from the deep ocean (Toggweiler et al., 2006; Denton et al., 2010). During the ACR, the SHW would have shifted northwards again, resulting in less  $\text{CO}_2$  ventilation and colder conditions in the SH mid-latitudes and Antarctica (Anderson et al., 2009).

An alternative hypothesis of SHW changes was brought forward by Lamy et al. (2010) for Holocene records of South America but the mechanism may also apply to the Last Termination (Kilian and Lamy, 2012). It was proposed, due to opposing precipitation records from the core and the northern boundary of the SHW, that the SHW belt did not shift latitudinally as a whole but rather that the wind belt expanded during colder periods (as observed during Austral winter today) and became more confined during warmer conditions (Austral summer). During colder conditions the northern margin of the belt experiences stronger SHW influence while the core of the belt becomes less influenced.

From existing proxy-data it is difficult to assess at which latitude the SHW were situated during LGM (Kohfeld et al., 2013), to which latitude they shifted at the onset of HS1, what their latitude was during the ACR and whether the wind belt shifted latitudinally or rather expanded and retracted.

Terrestrial data are mainly limited to southern South America and New Zealand and oceanic records usually lack a tightly constrained chronology due to changes in  $^{14}\text{C}$  reservoir ages (Siani et al., 2013). Furthermore, for a number of records, the proxies used mainly reflect temperature and/or precipitation changes,

which are not always directly linked to SHW intensity and hence their latitudinal position (Sime et al., 2013).

Anderson et al., 2009, observed higher opal fluxes during the Last Termination in cores situated south of the Polar Front (PF) from the Atlantic and Pacific sectors of the SO (Fig. 1A) and suggested that higher productivity was linked to the enhanced upwelling driven by a more southward position of the SHW during that period. Toggweiler et al. (2006) suggest that the wind belt shifted pole-ward towards their modern position at the onset of warming following the LGM. Based on our record, Kerguelen Islands (49°S) were less influenced by the SHW during HS1 and it is only at the onset of the OCR (13,600 cal yr BP) that intense westerly influence occurred. Taking into account that the archipelago today is situated in the core of the SHW, we propose that the wind belt was probably situated in a more southerly position during HS1, at least in the Indian Ocean basin. In a marine core situated near the Subtropical Front (STF) in the Atlantic Ocean (41°S, TNO57-21, Fig. 1A), the presence of warm planktonic foraminifera species (today occurring well north of the STF) during HS1 (c. 18,000–14,600 cal yr BP after Barker and Diz, 2014) indicates that this was the warmest period during the deglaciation, including the early Holocene, due to a more southerly position of the STF (Barker et al., 2009). A southward shift of the oceanic fronts could be related to a southward shift of the SHW during HS1, which is in agreement with our results from Kerguelen Islands. Moreover, temperatures seem to be highest near the onset of the ACR, coinciding with the very low accumulation rates due to high humification of the peat deposits in the Estacade record between 14,775 ( $2\sigma$  15,195–14,269) and 14,250 cal yr BP ( $2\sigma$  14,710–13,975).

In their higher resolution core of the Atlantic sector (TNO57-13, Fig. 1A) Anderson et al. (2009) observed that the increased opal flux of the Last Termination is interrupted by a lower opal flux that could correspond to the ACR. In the same basin (41°S, TNO57-21, Fig. 1A), Barker et al. (2009) interpreted a sudden increase in planktonic polar foraminifera species, near the onset of the ACR, as a sudden northward shift of the northern fronts associated with the Antarctic Circumpolar Current (ACC). A northward shift of the oceanic fronts should result in colder conditions in Kerguelen Islands at 49°S, with the PF likewise shifting northward encircling the archipelago with colder surface waters. The onset of slightly wetter conditions around 14,550 cal yr BP ( $2\sigma$  15,020–14,061) in the Estacade record could be an expression of lower temperatures due to a northward shift of the PF. However, as stated above (5.3.1), the uncertainty in our chronology at that time is rather large.

In the South East Pacific sector of the SO, based on a core along the Chilean margin (46°S, MD07-3088, Fig. 1A), the end of the first long Antarctic divergence upwelling period corresponding to the transition from HS1 to ACR is precisely dated to 14,620 cal yr BP ( $1\sigma$  14,870–14,610), thanks to the presence of a tephra layer (Siani et al., 2013). A pollen record from the same core shows a rapid northward shift of the SHW at the same time, bringing more precipitation to the area resulting in an expansion of Magellanic Moorland (Montade et al., 2013). This indicates that the site at 46°S was situated in the core of the SHW during the ACR. At the end of the ACR the wind belt shifted back south resulting in less intense SHW influence at 46°S and coinciding with the onset of the second upwelling period at 12,765 cal yr BP ( $1\sigma$  12,920–12,640) in the same record (Siani et al., 2013). Looking at the South West Pacific, in the Southern Alps of New Zealand, the culmination of late glacial glacier expansion and, in consequence, of the cooling is placed at  $12,970 \pm 300$  cal yr BP (Putnam et al., 2010), coinciding within dating uncertainties with the end of the ACR in the South East Pacific. From these data we can conclude that the most prominent change in the Estacade record occurring at 13,600 cal yr BP seems not to be registered in the South Pacific, indicating that this change

might be limited to the Indian Ocean basin. The Estacade record shows less intense SHW influence from 12,900 cal yr BP ( $2\sigma$  13,070–12,758) and onward, coinciding within chronological uncertainties with the end of the ACR. This decrease of SHW influence could reflect a pole-ward shift of the core of the wind belt in the Indian Ocean basin to a position south of Kerguelen Islands ( $49^\circ\text{S}$ ) similar to the pole-ward shift in the Pacific (south of  $46^\circ\text{S}$ ). About 11,650 cal yr BP ( $2\sigma$  12,006–11,304), warm, relatively dry and even less windy conditions occurred in the Estacade record, indicating a subsequent southward shift of the SHW at the early Holocene climate optimum. From a study of a peat sequence from Islas de los Estados (Atlantic sector of the SO,  $55^\circ\text{S}$ , Fig. 1A), combining both wind and precipitation proxies, more intense SHW during the ACR were inferred followed by a southward shift of the wind belt, with a position further south than  $55^\circ\text{S}$  attained by 12,200 cal yr BP (Björck et al., 2012). Both in the Atlantic and Indian sector of the SO, the SHW seem to have been situated south of their modern position during the Younger Dryas and the Holocene climate optimum.

Based on our record, Kerguelen Islands ( $49^\circ\text{S}$ ) were less influenced by the SHW during HS1 and YD. Taking into account that the archipelago is situated in the core of the SHW today we suggest that the SHW shifted south of Kerguelen Islands during Northern Hemisphere cold events (HS1 and YD) and shifted equator-ward during the ACR-OCR. Following Lamy et al. (2010), Kerguelen Islands should be less influenced by the SHW during the ACR-OCR as the belt was more expanded (Austral winter today), than during the warm SH events during HS1 and YD, which contradicts our results. However, the difference between summer and winter conditions of the wind belt is much less pronounced in the Indian Ocean than in South America and we want to stress that the hypothesis was brought forward based on Holocene records and has not been tested for the Last Termination. Moreover, it might be that the atmospheric circulation patterns were different in the different ocean basins as for example suggested by the deuterium excess records of the EDC and EDML ice cores (Stenni et al., 2011).

## 6. Conclusions

The Estacade peat record reveals clear changes during the Last Termination. Peat growth started 16,000 cal yr BP and continued until 13,600 cal yr BP suggesting relatively warm and humid conditions with slightly wetter conditions from 14,550 cal yr BP and onwards. A shift to a very wet and windy environment occurred 13,600 cal yr BP resulting in the formation of peat ponds and hence lacustrine-type deposits. We attribute this change to an intensification of the SHW, which coincides with the onset of the OCR as inferred from deuterium excess  $d$  in the EDC ice core. Lower temperatures during this period probably enhanced local wetness on the Estacade site. Around 12,900 cal yr BP, at the end of the ACR, pond/lake deposits give way to more peaty deposits suggesting slightly drier, less windy and probably warmer conditions. Kerguelen Islands became less influenced by the SHW although the wind tolerant cushion plant *A. selago* is still the dominant species in the area. About 11,650 cal yr BP warm, relatively dry and less windy conditions occurred with expansion of *A. magellanica* coinciding with the early Holocene climate optimum found in Antarctic ice cores.

Interestingly, the ACR is not clearly registered in the Estacade record. However, we do not have a straightforward temperature proxy. Whether the ACR coincides with a northward shift of the oceanic fronts combined with an equator ward shift of the SHW in the Indian sector of the SO is not clear yet. From our record, an intensification of the SHW was delayed until 13,600 cal yr BP. Based on the large error bars in the age model at 14,550 cal yr BP ( $2\sigma$

15,020–14,061) the onset of wetter conditions could theoretically be assigned to colder conditions at the onset of the ACR.

Our results could support the Toggweiler hypothesis: during LGM the SHW were well north of Kerguelen Islands and at the onset of HS1 a sudden southward shift of the wind belt (due to cold conditions in the northern hemisphere and a concurrent southward shift of the ITCZ) to south of the archipelago, creates the relatively warm and dry conditions for peat growth. During the OCR, the SHW moved northward and Kerguelen Islands were situated in the core of the wind belt. Subsequently a southward shift brings less intense SHW influence to Kerguelen Islands culminating in the early Holocene climate optimum. However, it seems that, during HS1, the SHW were not at the same latitude in the Indian sector of the SO as today. Moreover, we cannot exclude alternative scenarios of changing SHW. The Estacade record only starts 16,000 cal yr BP and does not cover the LGM making the assumptions about the LGM SHW latitude rather speculative.

## Acknowledgements

This research was made possible by the fantastic logistic support for fieldwork of the French Polar Institute (IPEV, Programme PEI-SACC – 448). Bart Klinck is warmly thanked for his invaluable help and never-ending enthusiasm in the field. Florian Adolphi, Wim Clymans, Daniel Conley, Guillaume Fontorbe, Patrick Frings, Git Klintvik Ahlberg, Raimund Muscheler and Anne Birgitte Nielsen from the Geology department, Lund University, Sweden are thanked for fruitful discussions and/or help with analyses. Malin Kylander (Stockholm University, Sweden) is thanked for the XRF core scanning. Ryszard Ochyra (Institute of Botany, Polish Academy of Sciences, Krakow, Poland) helped out with some bryophyte determinations and Françoise Hennion (CNRS, UMR ECOBIO, Université de Rennes 1, France) made reference material of *Lyallia kerguelensis* available.

Funding for NVdP was provided by Ghent University, Belgium (BOF-0111 2005) and the Swedish Research Council (VR-623-2009-7399, VR-349-2012-6278 and the LUCI Linnaeus grant). Grants for analyses and radiocarbon dating to NVdP from LUCI WP 3 and the Royal Physiographic Society in Lund, Sweden are greatly acknowledged. We thank the AMS ARTEMIS facility for  $^{14}\text{C}$  analyses made partly within the National CNRS-INSU service and partly through CEA participation. We also thank two anonymous reviewers for their valuable comments on an earlier version of the manuscript.

## Appendix A. Supplementary data

Supplementary data related to this article can be found at <http://dx.doi.org/10.1016/j.quascirev.2015.05.010>.

## References

- Aubert de la Rüe, E., 1962. Quelques particularités des tourbières de l'Archipel de Kerguelen. Leur répartition; leur structure et leur destruction. Rev. T.A.A.F 21, 12–30.
- Anderson, R.F., Ali, S., Bradtmiller, L.L., Nielsen, S.H.H., Fleisher, M.Q., Anderson, B.E., Burckle, L.H., 2009. Wind-driven upwelling in the Southern Ocean and the Deglacial Rise in atmospheric CO<sub>2</sub>. Science 323, 1443–1448.
- Andres, M.S., Bernasconi, S.M., McKenzie, J.A., Rohl, U., 2003. Southern Ocean deglacial record supports global Younger Dryas. Earth Planet. Sci. Lett. 216, 515–524.
- Barker, S., Diz, P., 2014. Timing of the descent into the last Ice Age determined by the bipolar seesaw. Paleoceanography 29, 2014PA002623.
- Barker, S., Diz, P., Vautravers, M.J., Pike, J., Knorr, G., Hall, I.R., Broecker, W.S., 2009. Interhemispheric Atlantic seesaw response during the last deglaciation. Nature 457, 1097–1102.
- Barrow, C.J., 1976. Palynological studies in South Georgia: I. Pollen and spore morphology of the native vascular species. Br. Antarct. Surv. Bull. 43, 63–75.

- Barrows, T.T., Lehman, S.J., Fifield, L.K., De Deckker, P., 2007. Absence of cooling in New Zealand and the Adjacent Ocean during the Younger Dryas Chronozone. 10.1126/science.1145873 *Science* 318, 86–89.
- Bellair, N., 1967. Sédimentologie et palynologie d'une tourbière de Kerguelen (Port-Christmas, Péninsule Loranchet). Faculté de Sciences de Paris, Paris, p. 58.
- Bennett, K.D., Haberle, S.G., Lumley, S.H., 2000. The Last Glacial-Holocene transition in Southern Chile. *Science* 290, 325–328.
- Biestler, H., Keppler, F., Putschew, A., Martínez-Cortizas, A., Petri, M., 2004. Halogen Retention, Organohalogenes, and the role of organic matter decomposition on Halogen Enrichment in two Chilean peat bogs. *Environ. Sci. Technol.* 38, 1984–1991.
- Björck, S., Rundgren, M., Ljung, K., Unkel, I., Wallin, Å., 2012. Multi-proxy analyses of a peat bog on Isla de los Estados, easternmost Tierra del Fuego: a unique record of the variable Southern Hemisphere Westerlies since the last deglaciation. *Quat. Sci. Rev.* 42, 1–14.
- Boyle, J.F., 2001. Inorganic geochemical methods in paleolimnology. In: Last, W.M., Smol, J.P. (Eds.), *Tracking Environmental Changes in Lake Sediments: Physical and Chemical Techniques*. Kluwer Academic Publishers, pp. 83–141.
- Broecker, W., 1998. Paleocirculation during the last deglaciation: a bipolar seesaw? *Paleoceanography* 13, 119–121.
- Bronk Ramsey, C., 2008. Deposition models for chronological records. *Quat. Sci. Rev.* 27, 42–60.
- Bronk Ramsey, C., 2009. Bayesian analysis of radiocarbon dates. *Radiocarbon* 51, 337–360.
- Bronk Ramsey, C., Lee, S., 2013. Recent and planned developments of the program OxCal. *Radiocarbon* 55, 720–730.
- Caseldine, C.J., Baker, A., Charman, D.J., Hendon, D., 2000. A comparative study of optical properties of NaOH peat extracts: implications for humification studies. *Holocene* 10, 649–658.
- Chambers, F.M., Beilman, D.W., Yu, Z., 2010/11. Methods for determining peat humification and for quantifying peat bulk density, organic matter and carbon content for palaeostudies of climate and peatland carbon dynamics. *Mires Peat* 7, Art. 7.
- Clymans, W., Barão, L., Van der Putten, N., Wastegård, S., Gísladóttir, G., Björck, S., Moine, B., Struyf, E., Conley, D.J., 2015. The contribution of tephra constituents during biogenic silica determination: implications for soil and paleoecological studies. *Biogeosci. Discuss.* 12, 3505–3545.
- Conley, D.J., Schelske, C.L., 2001. Biogenic silica. In: Smol, J.P., Birks, H.J.B., Last, W.M. (Eds.), *Tracking Environmental Change Using Lake Sediments, Terrestrial, Algal and Siliceous Indicators*, vol. 3. Kluwer Academic Publishers, Dordrecht, pp. 281–293.
- Demetrescu, E., 1999. The chlorococcalean alga *Botryococcus* and its significance in hydrocarbon exploration. *Geo-Eco-Marina* 4, 155–160.
- Denton, G.H., Anderson, R.F., Toggweiler, J.R., Edwards, R.L., Schaefer, J.M., Putnam, A.E., 2010. The Last Glacial Termination. *Science* 328, 1652–1656.
- Disnar, J.-R., Guillet, B., Keravis, D., Di-Giovanni, C., Sebag, D., 2003. Soil organic matter (SOM) characterization by Rock-Eval pyrolysis: scope and limitations. *Org. Geochem.* 34, 327–343.
- Espitalié, J., Laporte, J.L., Madec, M., Marquis, F., Leplat, P., Paulet, J., Boutefeu, A., 1977. Méthode rapide de caractérisation des roches mères, de leur potentiel pétrolier et de leur degré d'évolution. *Rev. l'Inst. Fr. Pétr.* 32, 23–42.
- Faegri, K., Kaland, P.E., Krzywinski, K., 1989. *Textbook of Pollen Analysis*. John Wiley and sons, Ltd, Chichester.
- Frenot, Y., Gloaguen, J.-C., Van de Vijver, B., Beyens, L., 1997. Datation de quelques sédiments tourbeux holocènes et oscillation glaciaires aux îles kerguelen. *C. R. Acad. Sci. Paris Ecol.* 320, 567–573.
- Frenot, Y., Gloaguen, J.-C., Massé, L., Lebouvier, M., 2001. Human activities, ecosystem disturbance and plant invasions in subantarctic Crozet, Kerguelen and Amsterdam Islands. *Biol. Conserv.* 101, 33–50.
- Gautier, I., Weis, D., Mennessier, J.-P., Vidal, P., Giret, A., Loubet, M., 1990. Petrology and geochemistry of the Kerguelen Archipelago basalts (South Indian Ocean): evolution of the mantle sources from ridge to intraplate position. *Earth Planet. Sci. Lett.* 100, 59–76.
- Giret, A., Weis, D., Grégoire, M., Mattielli, N., Moine, B., Michon, G., Scoates, J., Tourpin, S., Delpoch, G., Gerbe, M.C., Doucet, S., Ethien, R., Cottin, J.Y., 2003. L'Archipel de Kerguelen: les plus vieilles îles dans le plus jeune océan. *Géologues* 137, 23–40.
- Grasshoff, K., Ehrhardt, M., Kremling, K., 1983. *Methods of Sea Water Analysis*. Verlag, Chemie, p. 314.
- Grimm, E.C., 2004. *TGView, 2.0.2*. ed. Illinois State Museum Research Collection Center, Springfield.
- Guy-Ohlsen, D., 1992. *Botryococcus* as an aid in the interpretation of palaeoenvironment and depositional processes. *Rev. Palaeobot. Palynol.* 71, 1–15.
- Hall, K., 1984. Evidence in favour of an extensive ice cover on sub-Antarctic Kerguelen Island during the Last Glacial. *Palaeogeogr. Palaeoclimatol. Palaeoecol.* 47, 225–232.
- Hammer, Ø., Harper, D.A.T., Ryan, P.D., 2001. *PAST: Paleontological statistics software package for education and data analysis*. *Palaeontol. Electron.* 4 (1), 9.
- Hodgson, D.A., Graham, A.G.C., Roberts, S.J., Bentley, M.J., Cofaigh, C.O., Verleyen, E., Vyverman, W., Jomelli, V., Favier, V., Brunstein, D., Verfaillie, D., Colhoun, E.A., Saunders, K.M., Selkirk, P.M., Mackintosh, A., Hedding, D.W., Nel, W., Hall, K., McGlone, M.S., Van der Putten, N., Dickens, W.A., Smith, J.A., 2014. Terrestrial and submarine evidence for the extent and timing of the Last Glacial Maximum and the onset of deglaciation on the maritime-Antarctic and sub-Antarctic islands. *Quat. Sci. Rev.* 100, 137–158.
- Hogg, A.G., Hua, Q., Blackwell, P.G., Niu, M., Buck, C.E., Guilderson, T.P., Heaton, T.J., Palmer, J.G., Reimer, P.J., Reimer, R.W., Turney, C.S.M., Zimmerman, S.R.H., 2013. *SHCal13 Southern Hemisphere Calibration, 0–50,000 Years cal BP*.
- Jacob, J., Disnar, J.-R., Boussafir, M., Sifeddine, A., Turcq, B., Albuquerque, A.L.S., 2004. Major environmental changes recorded by lacustrine sedimentary organic matter since the last glacial maximum near the equator (Lagoa do Caço, NE Brazil). *Palaeogeogr. Palaeoclimatol. Palaeoecol.* 205, 183–197.
- Janssens, J.A., 1983. A quantitative method for stratigraphic analysis of bryophytes in Holocene peat. *J. Ecol.* 71, 189–196.
- Johnson, T.C., Brown, E.T., Shi, J., 2011. Biogenic silica deposition in Lake Malawi, East Africa over the past 150,000 years. *Palaeogeogr. Palaeoclimatol. Palaeoecol.* 303, 103–109.
- Kilian, R., Lamy, F., 2012. A review of Glacial and Holocene paleoclimate records from southernmost Patagonia (49–55°S). *Quat. Sci. Rev.* 53, 1–23.
- Kohfeld, K.E., Graham, R.M., de Boer, A.M., Sime, L.C., Wolff, E.W., Le Quéré, C., Bopp, L., 2013. Southern Hemisphere westerly wind changes during the Last Glacial Maximum: paleo-data synthesis. *Quat. Sci. Rev.* 68, 76–95.
- Kylander, M.E., Lind, E.M., Wastegård, S., Löwemark, L., 2012. Recommendations for using XRF core scanning as a tool in tephrochronology. *Holocene* 22, 371–375.
- Lafargue, E., Marquis, F., Pillot, D., 1998. Rock-Eval 6 applications in hydrocarbon exploration, production, and soil contamination studies. *Rev. l'Inst. Fr. Pétr.* 53, 421–437.
- Lamy, F., Kilian, R., Arz, H.W., Francois, J.-P., Kaiser, J., Prange, M., Steinke, T., 2010. Holocene changes in the position and intensity of the southern westerly wind belt. *Nat. Geosci.* 3, 695–699.
- Lewis-Smith, R.L., 1984. *Terrestrial plant biology of the sub-Antarctic and Antarctic*. In: Laws, R.M. (Ed.), *Antarctic Ecology*. Academic Press, London, pp. 61–162.
- Liu, X., Colman, S., Brown, E., Minor, E., Li, H., 2013. Estimation of carbonate, total organic carbon, and biogenic silica content by FTIR and XRF techniques in lacustrine sediments. *J. Paleolimnol.* 50, 387–398.
- Lowe, J.J., Rasmussen, S.O., Björck, S., Hoek, W.Z., Steffensen, J.P., Walker, M.J.C., Yu, Z.C., 2008. Synchronisation of palaeoenvironmental events in the North Atlantic region during the Last Termination: a revised protocol recommended by the INTIMATE group. *Quat. Sci. Rev.* 27, 6–17.
- Masson, V., Vimeux, F., Jouzel, J., Morgan, V., Delmotte, M., Ciais, P., Hammer, C., Johnsen, S., Lipenkov, V.Y., Mosley-Thompson, E., 2000. Holocene climate variability in Antarctica based on 11 ice-core isotopic records. *Quat. Res.* 54, 348–358.
- Montade, V., Combourieu Nebout, N., Kissel, C., Haberle, S.G., Siani, G., Michel, E., 2013. Vegetation and climate changes during the last 22,000 yr from a marine core near Taitao Peninsula, southern Chile. *Palaeogeogr. Palaeoclimatol. Palaeoecol.* 369, 335–348.
- Nougier, J., 1970. Contribution à l'étude géologique et géomorphologique des îles Kerguelen. *C.N.F.R.A.* 27, p. 440.
- Putnam, A.E., Denton, G.H., Schaefer, J.M., Barrell, D.J.A., Andersen, B.G., Finkel, R.C., Schwartz, R., Doughty, A.M., Kaplan, M.R., Schluchter, C., 2010. Glacier advance in southern middle-latitudes during the Antarctic Cold Reversal. *Nat. Geosci.* 3, 700–704.
- Roos-Barraclough, F., van der Knaap, W.O., van Leeuwen, J.F.N., Shoty, W., 2004. A Late-glacial and Holocene record of climatic change from a Swiss peat humification profile. *Holocene* 14, 7–19.
- Sandgren, P., Snowball, I.F., 2001. Application of mineral techniques to paleolimnology. In: Last, W.M., Smol, J.P. (Eds.), *Tracking Environmental Changes in Lake Sediments: Physical and Chemical Techniques*. Kluwer Academic Publishers, pp. 217–237.
- Shoty, W., 1997. Atmospheric deposition and mass balance of major and trace elements in two oceanic peat bog profiles, northern Scotland and the Shetland Islands. *Chem. Geol.* 138, 55–72.
- Siani, G., Michel, E., De Pol-Holz, R., DeVries, T., Lamy, F., Carel, M., Isguder, G., Dewilde, F., Laurantou, A., 2013. Carbon isotope records reveal precise timing of enhanced Southern Ocean upwelling during the last deglaciation. *Nat. Commun.* 4.
- Sime, L.C., Kohfeld, K.E., Le Quéré, C., Wolff, E.W., de Boer, A.M., Graham, R.M., Bopp, L., 2013. Southern Hemisphere westerly wind changes during the Last Glacial Maximum: model-data comparison. *Quat. Sci. Rev.* 64, 104–120.
- Sommer, M., Kaczorek, D., Kuzyakov, Y., Breuer, J., 2006. Silicon pools and fluxes in soils and landscapes — a review. *J. Plant Nutr. Soil Sci.* 169, 310–329.
- Steig, E.J., Brook, E.J., White, J.W.C., Sucher, C.M., Bender, M.L., Lehman, S.J., Morse, D.L., Waddington, E.D., Clow, G.D., 1998. Synchronous climate changes in Antarctica and the North Atlantic. *Science* 282, 92–95.
- Stenni, B., Masson-Delmotte, V., Johnsen, S., Jouzel, J., Longinelli, A., Monnin, E., Röthlisberger, R., Selmo, E., 2001. An oceanic cold reversal during the last deglaciation. *Science* 293, 2074–2077.
- Stenni, B., Masson-Delmotte, V., Selmo, E., Oerter, H., Meyer, H., Röthlisberger, R., Jouzel, J., Cattani, O., Falourd, S., Fischer, H., Hoffmann, G., Iacumin, P., Johnsen, S.J., Minster, B., Udisti, R., 2010. The deuterium excess records of EPICA Dome C and Dronning Maud Land ice cores (East Antarctica). *Quat. Sci. Rev.* 29, 146–159.
- Stenni, B., Buiron, D., Frezzotti, M., Albani, S., Barbante, C., Bard, E., Barnola, J.M., Baroni, M., Baumgartner, M., Bonazza, M., Capron, E., Castellano, E., Chappellaz, J., Delmonte, B., Falourd, S., Genoni, L., Iacumin, P., Jouzel, J., Kipfstuhl, S., Landais, A., Lemieux-Dudon, B., Maggi, V., Masson-Delmotte, V., Mazzola, C., Minster, B., Montagnat, M., Mulvaney, R., Narcisi, B., Oerter, H., Parrenin, F., Petit, J.R., Ritz, C., Scarchilli, C., Schilt, A., Schupbach, S., Schwander, J., Selmo, E., Severi, M., Stocker, T.F., Udisti, R., 2011. Expression of

- the bipolar see-saw in Antarctic climate records during the last deglaciation. *Nat. Geosci.* 4, 46–49.
- Toggweiler, J.R., Russell, J.L., Carson, S.R., 2006. Midlatitude westerlies, atmospheric CO<sub>2</sub>, and climate change during the ice ages. *Paleoceanography* 21, PA2005.
- Unkel, I., Fernandez, M., Björck, S., Ljung, K., Wohlfarth, B., 2010. Records of environmental changes during the Holocene from Isla de los Estados (54.4°S), southeastern Tierra del Fuego. *Glob. Planet. Change* 74, 99–113.
- Van der Putten, N., Stieperaere, H., Verbruggen, C., Ochyra, R., 2004. Holocene palaeoecology and climate history of South Georgia (sub-Antarctica) based on a macrofossil record of bryophytes and seeds. *Holocene* 14, 382–392.
- Van der Putten, N., Verbruggen, C., Ochyra, R., de Beaulieu, J.-L., De Dapper, M., Spassov, S., Hus, J., Thouveny, N., 2009. Peat bank growth, Holocene palaeoecology and climate history of South Georgia (sub-Antarctica), based on a botanical macrofossil record. *Quat. Sci. Rev.* 28, 65–79.
- Van der Putten, N., Verbruggen, C., Ochyra, R., Verleyen, E., Frenot, Y., 2010. Subantarctic flowering plants: pre-glacial survivors or post-glacial immigrants? *J. Biogeogr.* 37, 582–592.
- Van der Putten, N., Mauquoy, D., Verbruggen, C., Björck, S., 2012a. Subantarctic peatlands and their potential as palaeoenvironmental and palaeoclimatic archives. *Quat. Int.* 268, 65–76.
- Van der Putten, N., Verbruggen, C., De Beaulieu, J.L., Björck, S., Barrow, C.J., Frenot, Y., 2012b. Is palynology a credible climate proxy in the Subantarctic? *Holocene* 22, 1113–1121.
- Veres, D., Bazin, L., Landais, A., Toyé Mahamadou Kele, H., Lemieux-Dudon, B., Parrenin, F., Martinerie, P., Blayo, E., Blunier, T., Capron, E., Chappellaz, J., Rasmussen, S.O., Severi, M., Svensson, A., Vinther, B., Wolff, E.W., 2013. The Antarctic ice core chronology (AICC2012): an optimized multi-parameter and multi-site dating approach for the last 120 thousand years. *Clim. Past* 9, 1733–1748.
- Wagstaff, S.J., Hennon, F., 2007. Evolution and biogeography of *Lyallia* and *Hectorella* (Portulacaceae), geographically isolated sisters from the Southern Hemisphere. *Antarc. Sci.* 19, 417–426.
- Williams, P.W., King, D.N.T., Zhao, J.X., Collerson, K.D., 2005. Late Pleistocene to Holocene composite speleothem 18O and 13C chronologies from South Island, New Zealand—did a global Younger Dryas really exist? *Earth Planet. Sci. Lett.* 230, 301–317.
- Young, S.B., Schofield, E.K., 1973. Pollen evidence for Late Quaternary climate changes on Kerguelen Island. *Nature* 245, 311–312.